Methyldisulfide groups enable the direct connection of air-stable metal bis(terpyridine) complexes to gold surfaces

Christina D.M. Trang, Thomas Saal, and Michael S. Inkpen*

Department of Chemistry, University of Southern California, Los Angeles, CA 90089, United States

E-mail: inkpen@usc.edu

ABSTRACT

We show that a new terpyridine ligand comprising a directly-connected methyldisulfide group (**tpySSMe**) can be used to prepare a modular series of metal bis(terpyidine) complexes, [M(**tpySSMe**)$_2$](PF$_6$)$_2$ (M = Fe, Co, Zn), suitable for the functionalization of metal surfaces. Critically, we find these complexes are air-stable in solution for >7 d, in stark contrast to their thiol-substituted analogues, [M(**tpySH**)$_2$](PF$_6$)$_2$ (M = Fe, Co), which decompose in <1 d. While **CoSH** has previously been utilized in several important studies, we explicitly detail its synthesis and characterization here for the first time. We subsequently probe the electrochemical properties of [M(**tpySSMe**)$_2$](PF$_6$)$_2$ in solution, showing that the (electro)chemical reactions associated with disulfide reduction significantly increase the complexity of the voltammetric response. In preliminary surface voltammetry studies, we confirm that **CoSS** and **FeSS** form solution-stable self-assembled monolayers (SAMs) on gold with comparable electrochemical properties to those formed from **CoSH**. Taken together, this work provides a robust foundation for future studies of this prominent class of complexes as redox-active components of SAMs or single-molecule junctions.

INTRODUCTION

In seminal reports of unusual charge transport and magnetic phenomena, several studies have focused on self-assembled monolayers (SAMs) or molecular junctions comprising metal bis(terpyridine) complexes with *directly connected* sulfur-based anchors, $\mathbf{[M(L)_2]^{2+}}$ (**Figure 1a**). $\mathbf{[M(L)_2]^{2+}}$ complexes used include those with M = Co, Zn, and Ru, where L is tpySAc = 2,2':6',2''-terpyridine-4'-thioacetate, **tpySH** = 2,2':6',2''-terpyridine-4'-thiol, or tpy = 2,2':6',2''-terpyridine.[1–4] In addition to their demonstrated utility, we also recognize that $\mathbf{[M(L)_2]^{2+}}$ are potentially interesting redox-active molecular "platforms" – pre-formed components with bulky lateral dimensions that dictate the close-packed monolayer structure.[3,5] Such platforms may be used to introduce different functional species and/or free volume into a SAM without disrupting the underlying surface assembly process, a long-standing challenge in the field. Remarkably, however, no explicit synthetic procedures or characterization details for the aforementioned $\mathbf{[M(L)_2]^{2+}}$ compounds are provided in the noted works or their referenced articles, significantly impeding further developments in this area.

We suggest that the direct attachment of anchor groups to pre-formed metal bis(terpyridine) monolayer components provides specific advantages for controlling the organization and composition of SAMs comprising these functional units. Previously reported surface attachment strategies using extended, pendant surface tethers[6–10] introduce additional degrees of freedom that can complicate molecular packing at the nanoscale.[11,12] While stepwise surface-based synthetic reactions have been utilized to construct similar complexes *in situ*,[13–16] here it may be challenging to control the extent to which different ligands and metals are introduced into such SAMs as a result of the varying kinetics of metal-ligand complexation and intramolecular steric effects within the surface layer.[17–19]

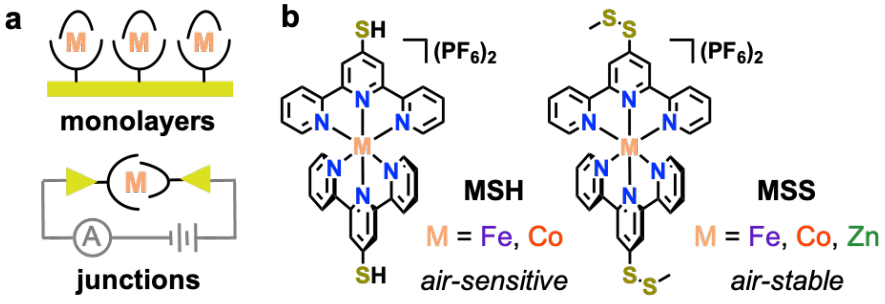

Figure 1. (a) Transition metal bis(terpyridine) complexes have been frequently targeted as modular components of self-assembled monolayers (SAMs) or molecular-scale junctions. **(b)** Molecular structures of $[M(\mathbf{tpySH})_2](PF_6)_2$ (**MSH**) and $[M(\mathbf{tpySSMe})_2](PF_6)_2$ (**MSS**). ^1H NMR spectroscopic studies reveal **MSH** complexes are air-sensitive in solution, in contrast to their air-stable **MSS** analogues.

Potential challenges in resolving preparative methods for $\mathbf{[M(L)_2]^{2+}}$ may be convoluted with the reported instabilities of related compounds in air. A detailed 2008 study of $[Fe(\mathbf{tpySH})_2](PF_6)_2$ (**FeSH**) found it was stable for only ~1 d in solution, forming a tetrameric product through disulfide oxidation.[20] Deprotonation of **FeSH** was also shown by ^{1}H NMR, UV-vis, and IR spectroscopy to produce a highly air-sensitive thione complex $Fe(tpy{=}S)_2$.[20] Few characterized examples of other **tpySH**-containing metal bis(terpyridine) complexes (with M = Ru[21] and Ni[22]) have been described. While thiol-protected ligands such as tpySAc[23] could offer routes to stable precursor complexes, deprotection of the corresponding $[M(tpySAc)_2](PF_6)_2$ complexes (e.g., with NBu_4OH, NBu_4F) is anticipated to result in unstable thione species via the intermediate thiolate. Such deprotection strategies are likely further complicated by counterion exchange by OH^-/F^-, or counterion loss from the charge neutral thione. New approaches are urgently needed to access air-stable $\mathbf{[M(L)_2]^{2+}}$ complexes capable of binding to metal surfaces. In this work, we demonstrate that complexes comprising a new methyldisulfide (-SSMe)-functionalized ligand (**MSS**; M = Fe, Co, Zn) are both synthetically accessible and air-stable in solution, in stark contrast to **CoSH** which rapidly decomposes when exposed to air (**Figure 1b**). Preliminary surface voltammetry studies reveal **CoSS** forms solution-stable SAMs with comparable surface coverage and redox peak widths to **CoSH**, confirming that the -SSMe group serves as a competent anchor for binding these complexes to metal surfaces.

RESULTS AND DISCUSSION

We explicitly target -SSMe groups as alternative, chemically robust, sulfur-based surface linkers for functional metal bis(terpyridine) complexes for several key reasons. Critically, Whitesides *et al.* have shown dialkyldisulfides can spontaneously form SAMs of comparable composition to those constructed from analogous alkylthiols,[24] and it has recently been determined that disulfide groups cleave during solution-based scanning tunneling microscope-based break junction studies to form covalent gold-sulfur bonded single-molecule junctions.[25] We further reasoned that disulfides would exhibit good chemical compatibility with terpyridine coordination chemistry given the numerous examples of metal complexes comprising intact 4,4'-dipyridyldisulfide ligands.[26] Use of an asymmetric disulfide, rather than a symmetric ligand such as terpy-SS-terpy,[27] would avoid the formation of coordination oligomers/polymers at homoleptic metal centers. We recognize that such asymmetrical disulfides will produce mixed SAMs containing dissociated, surface-bound -SMe, with

compositions that likely deviate from a 1:1 ratio.[28] However, we anticipate that domains of bound -SMe species would exhibit minimal stabilizing lateral interactions due to the short alkane component,[28–30] ensuring that the terpyridine complex is maximally competitive for surface binding. We also anticipate that any residual -SMe is small enough to bind within the area occupied by the complex on the surface. The practical utility of the -SSMe group in this context is evaluated below through surface voltammetry experiments.

We prepared the new ligand 4'-(methyldisulfide)-2,2':6',2''-terpyridine (**tpySSMe**) in two steps from 4'-chloro-2,2':6',2''-terpyridine in 79% overall yield (**Figure 2a**). Our approach involved the formation of **tpySH** via nucleophilic attack by sodium hydrosulfide,[27] which is then methylthiolated using S-methyl methanethiosulfonate.[31] The X-ray crystal structure of this ligand is shown in **Figure 2b**. Following established methods,[32–34] reactions of **tpySSMe** with the appropriate M^{2+} salt at room temperature provided the corresponding [M(**tpySSMe**)$_2$]$(PF_6)_2$ complexes for M = Fe (**FeSS**), Co (**CoSS**), and Zn (**ZnSS**) (**Figure 2c**). ^{1}H NMR spectra reveal that **MSS** are stable in MeCN-d_3 solutions for ≥7 d, in stark contrast to the ~1 d reported for **FeSH** (see **SI, Figure S16** for representative **FeSS** spectra). For completeness, we obtained not only the ^{1}H NMR spectrum for the paramagnetic d^7 Co(II) **CoSS** complex,[35] but also the spectrum of the corresponding diamagnetic Co(III) d^6 species (**CoSS^{3+}**) after chemical oxidization of **CoSS** with $AgPF_6$. X-ray crystal structures of **FeSS**, **CoSS**, and **ZnSS** show the expected homoleptic metal complexes with distorted octahedral geometries and intact disulfide groups (**Figure 2d-f**). Small changes in the average 4-carbon-4"-carbon distances of 9.256, 9.372, and 9.432 Å, respectively (denoted by † and ‡ for **FeSS**), correlate with the average M-N bond distances for each compound (Fe-N = 1.947(8), Co-N = 2.016(5), Zn-N = 2.152(4) Å). As expected, the structure and dimensions of these complexes are not appreciably altered by varying the central metal ion, an important consideration in the pursuit of well-mixed multicomponent SAMs.

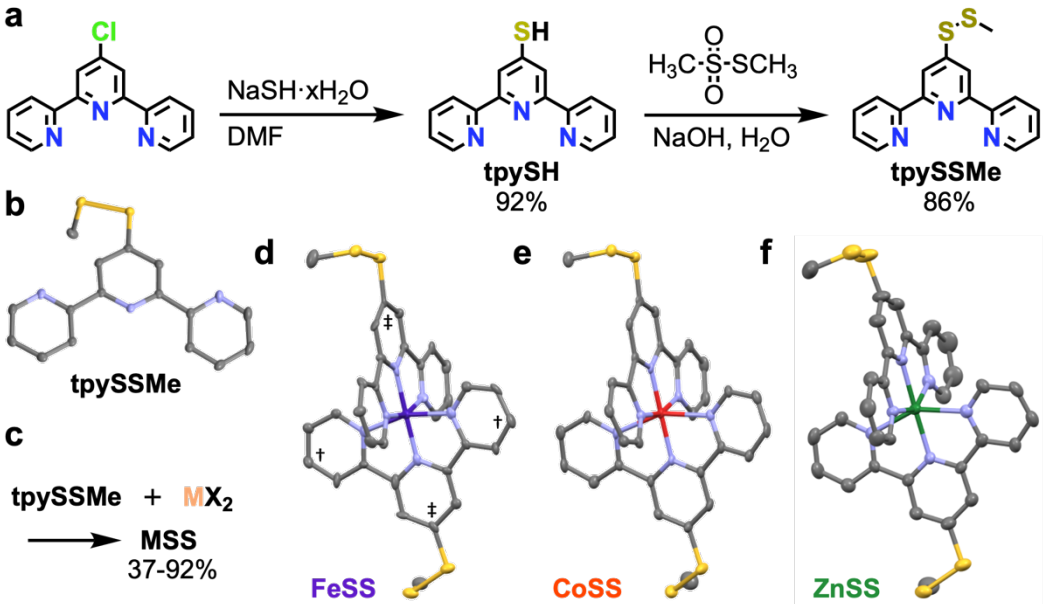

Figure 2. (a) Two-step synthetic route to **tpySSMe** ligand. **(b)** X-ray crystal structure of **tpySSMe**. **(c)** Synthetic route to disulfide-functionalized complexes (M = Fe, Co, Zn) using M^{2+} salts (see the **SI** for detailed synthetic methods). **(d-f)** X-ray crystal structures of **FeSS**, **CoSS**, and **ZnSS**, respectively. Small changes in the average 4-carbon-4"-carbon distances (denoted by † and ‡ for **FeSS**) correlate with the average M-N bond distances for each compound. Hydrogen atoms, solvent, and counter ions (where relevant) are omitted from all crystal structures for clarity (50% probability ellipsoids, S = yellow, N = blue, C = grey, Fe = purple, Co = orange, Zn = green). Selected structural parameters are provided in the **SI, Tables S1-8**.

With routes to air-stable **MSS** complexes established, we sought to develop a robust synthesis of **CoSH** to determine whether this (in addition to **FeSH**) exhibits air-instability in solution. Following a method analogous to that used for **CoSS** (see the **SI** for detailed synthetic methods), the reaction of $CoCl_2 \cdot 6H_2O$ with **tpySH** under an inert nitrogen atmosphere initially provided an orange solution, but ultimately yielded a black solid with an intractable ^{1}H NMR spectrum after work up in air. Pure **CoSH** was isolated as a dark orange powder only with rigorous exclusion of air during synthesis and purification, as confirmed by ^{1}H NMR spectroscopy, mass spectrometry, and elemental analysis. Notably, this complex was observed to decompose in solution after air-exposure in <1 d, as indicated by significant changes in its paramagnetic ^{1}H NMR spectrum (**SI, Figure S17**). This clearly indicates that **MSH** (at least for M = Fe, Co) should only be utilized in SAMs or molecular junctions if these can be formed and studied under an inert atmosphere. While the -SH group that contacts the surface may be stabilized, in air the unbound -SH groups may form disulfide-linkages between adjacent molecules or form unstable thione-based complexes if exposed to basic environments (see

above discussion of **FeSH** solution stability). We note that performing solution-based molecular junction measurements with rigorous exclusion of air is not trivial, requiring custom-built instrumentation that is not yet widely available.[36]

We subsequently assessed the influence of the redox active -SSMe group[37] on the electrochemical properties and stability of **MSS** complexes in solution. In **Figure 3a-c** we plot overlaid solution cyclic voltammograms of **FeSS**, **CoSS**, and **ZnSS**, respectively. For potential windows that do not extend below approximately −1.4 V vs. the FcH/$[FcH]^+$ redox couple, we find that both **FeSS** and **CoSS** show single reversible redox events ($i_{pa}/i_{pc} \approx 1$, $i_p \propto V_s^{1/2}$; selected data is provided in the **SI, Table S9**). We assign these features to the $M^{2+/3+}$ couple, as their redox potentials align well with the same processes reported for the parent species (**SI, Figure S2**, **Table S9**). These solution studies indicate that SAMs comprising **FeSS** or **CoSS** may be unambiguously characterized by surface voltammetry at potentials positive of the disulfide, or anticipated gold-sulfur,[38] reduction processes, as we confirm below. **ZnSS** voltammograms are featureless across this potential range.

When the electrochemical window is extended to more reducing potentials, we observe a new irreversible reduction feature with a peak potential around −1.5 V for all compounds. This feature is notably absent in voltammograms of the parent species (**Figure S2**), and significantly increases the complexity of the voltammetric response. Through comparison to voltammograms of the free **tpySSMe** ligand (**SI, Figure S3a** and **Table S10**), and other aspects of the **MSS** voltammograms (see below), we tentatively attribute this feature to the 1 or 2 e^- reduction of a disulfide group. This process is thought to facilitate heterolytic or homolytic S-S bond cleavage, respectively, resulting in formation of the corresponding thiyl radical and/or thiolate species (i-a or i-b, **Figure 3e**).[37,39,40] In **MSS**, metal-coordination appears to increase the potential of disulfide reduction by approximately +0.7 V (**SI, Table S10**). When scanning to even greater reducing potentials we observe additional features we attribute to the reversible ligand-based reductions previously assigned for $[M(tpy)_2]^{2+}$, now shifted to lower potentials as would be expected following the *in situ* generation of an electron-rich thiolate group.[41]

Any thiolate species formed from the reduction of a disulfide in **MSS** may be subsequently oxidized to thiyl radicals upon cycling back to more positive potentials. These radicals can then combine to form a mixture of symmetrical and asymmetrical disulfides (iii, **Figure 3e**).[37] Indeed, solution voltammograms that show disulfide reduction waves also exhibit new features between −0.3 and 0.9 V that we attribute to thiolate oxidation processes (ii, **Figure 3a-c**). In **Figure S3**, we present solution voltammograms for **tpySSMe** and dimethyldisulfide

(**MeSSMe**) for comparison. The potentials for thiolate oxidation appear to be sensitive to the group bound to sulfur and the surrounding electrolytic environment (**Table S10**).

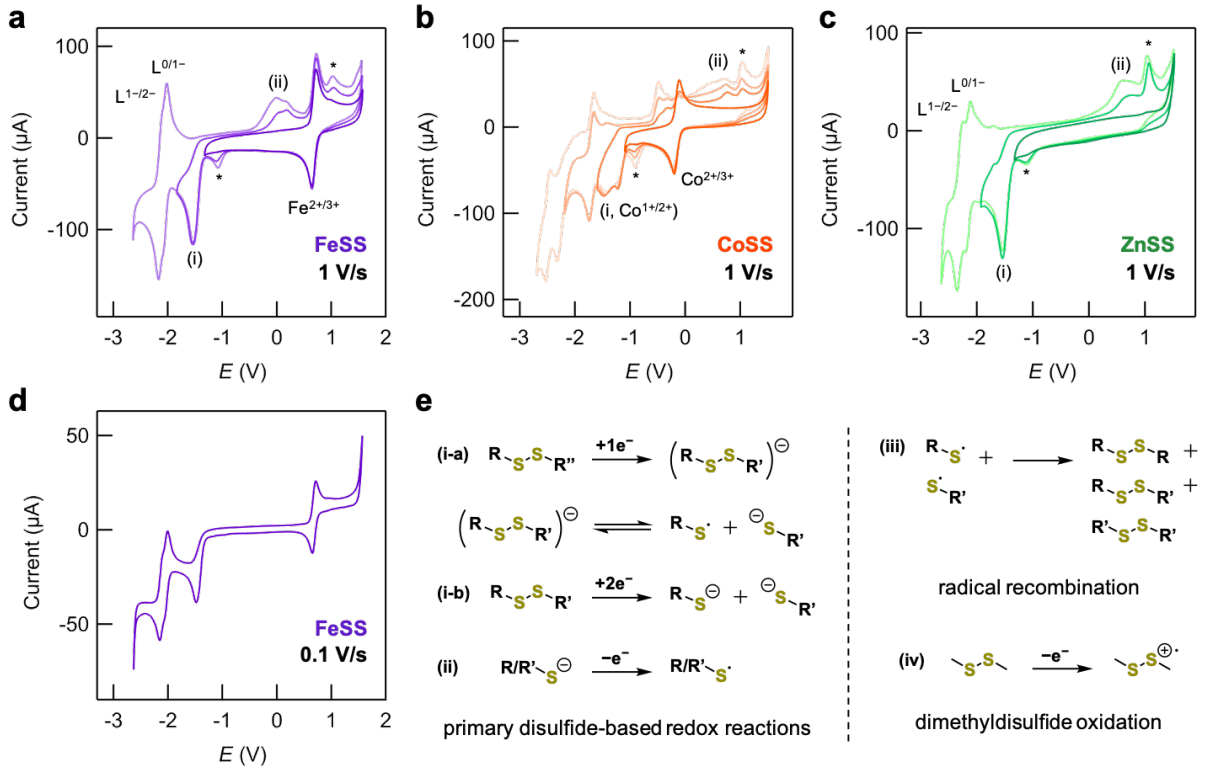

Figure 3. (a) Overlaid cyclic voltammograms of **FeSS** in MeCN−0.1 M $^{n}Bu_4NPF_6$, extended to different reducing potentials. We tentatively attribute the new irreversible wave at −1.5 V (i), absent for the parent complex, to the 2 × 1 e^- reduction of each disulfide group (see discussion). This reduction is associated with additional redox processes observed when scanning back to positive potentials. Here, (ii) labels mark features we associate with the thiolate oxidation processes shown in (e), "*" indicates features we propose result from dimethyldisulfide oxidation (scheme (iv) in (e), voltammograms of dimethyldisulfide are shown in **Figure S3**). **(b,c)** Analogous overlaid cyclic voltammograms for **CoSS** and **ZnSS**. For **CoSS**, we observe that the $Co^{2+/3+}$ oxidation shifts from −0.109 to −0.486 mV after extension of the potential window to include disulfide reduction. It is to be expected that a complex bearing an electron-donating thiolate functionality ($-S^-$; Hammett *para*-substituent constant, $\sigma_p = -1.21$) would be more easily oxidized than the same complex with a -SSMe group ($\sigma_p = 0.13$).[41] **(d)** A cyclic voltammogram of **FeSS** obtained at a slower scan rate (0.1 V/s). This shows that the additional redox processes and reactions associated with disulfide reduction are absent, confirming these originate from solution-based products that diffuse away from the electrode over extended timescales. **(e)** An overview of reaction schemes discussed in (a).

For all **MSS** complexes, we also observe a small irreversible oxidation feature ~1 V, commensurate with an irreversible reduction at ~−1V (waves marked "*" in **Figure 3a-c**).

Notably, the potential of this oxidation feature is ~constant and the same as that of an irreversible oxidation process in the voltammogram of **MeSSMe** (**Figure S3**, **Table S10**). We therefore attribute these events in voltammograms of **MSS** to oxidation of **MeSSMe** (scheme iv, **Figure 3e**; where **MeSSMe** is formed through recombination of two methylthiyl radicals) and reduction of the product(s) formed from its reactive radical cation. At slower scan rates the additional redox features associated with thiolate and **MeSSMe** oxidation are no longer observed in the voltammogram, confirming that they are associated with products of disulfide reduction that diffuse away from the electrode over extended timescales (**Figure 3d**). While identification of all electrochemically generated compounds is beyond the scope of this work, we note that the products formed from reactions of disulfide radical cations are considered dependent on the electrolyte, solvent, or impurities present. Reported species include: trisulfides ($[R_3S_3]^+$), following disulfide radical dimerization to a $[R_4S_4]^{2+}$ intermediate that subsequently undergoes nucleophilic attack by a neutral disulfide;[42] and protonated amides ($RSN^+H_2C(O)CH_3$), after reaction of $[RS]^+$ with MeCN solvent and adventitious water.[43]

Further examination of the disulfide reduction and $M^{2+/3+}$ oxidation features for **FeSS** shows that the ratio of their peak areas is ~2:1. This suggests that each disulfide undergoes a 1 e^- reduction, or that a 2 e^- reduction takes place at only one of the disulfide groups on this complex. For **FeSS** the difference between the peak and half-peak potentials ($E_p - E_{p/2} = 56.5/n$, where n is the number of electrons in the redox process) for the $Fe^{2+/3+}$ wave is ~65 mV, close to the expected value for a 1 e^- process.[44] However, for **FeSS** and **ZnSS** the disulfide reduction wave has $E_p - E_{p/2}$ = 103 and 94 mV, respectively. This peak broadening suggests the feature corresponds to two closely overlapping 1 e^- processes, rather than a concerted 2 e^- reduction. Accordingly, we tentatively assign this feature to the 1 e^- reduction of each disulfide group, with the first and second reductions occurring at different potentials given that it is energetically more favorable to add an electron to a complex having a charge of 2+ than 1+. Further evidence for this assignment may be provided in subsequent studies of related compounds, for example, through the electrochemical characterization of a heteroleptic complex comprising a single disulfide group. We note that for **CoSS** the disulfide reduction and $Co^{1+/2+}$ features are convoluted, which severely complicates their analysis.

To evaluate the capability of **MSS** to form SAMs on gold, we exposed mechanically polished gold disc electrodes to 1 mM solutions of **FeSS** and **CoSS** in MeCN for ≥18 h. In **Figure 4b**, we present overlaid representative surface cyclic voltammograms for these electrodes measured in CH_2Cl_2–0.1 M $^nBu_4NPF_6$. In each case, reversible redox features

indicative of adsorbed **MSS** are clearly observed at potentials ~50-140 mV positive of the potential of the corresponding $M^{2+/3+}$ couple measured in solution (overlaid solution voltammograms are provided in **Figure 4a** for comparison; i_{pa}/i_{pc} close to 1 for redox active SAMs, $i_p \propto V_s$; selected data is provided in the **SI, Table S11**). A comparable voltammetric response is observed for **CoSS** SAMs prepared on thermally evaporated gold electrodes, indicating the electrochemical properties and surface composition of these SAMs is broadly independent of the electrode surface roughness (**SI, Figure S4a**). The characteristic double-layer capacitance of **MSS** SAMs is lower than that suggested by the voltammograms in **Figure 3b**, as can be seen for voltammograms obtained from the same electrode when scanning to potentials below the oxidative limit (**SI, Figure S4b**). Similar surface voltammograms are observed for **CoSH** and **CoSS** SAMs prepared under an inert atmosphere (**Figure 4c**), indicating monolayers of comparable surface coverage and structure are formed using either –SH or –SSMe functionalized precursors. This result clearly shows that that the use of -SSMe groups, despite generating surface adsorbed -SMe, does not impede the adsorption of these terpyridine complexes on gold electrodes.

We find that the intensity of $M^{2+/3+}$ features for **MSS** SAMs does not significantly decrease upon repeated potential cycling, or after immersion in CH_2Cl_2/MeCN for 1 h, showing that these systems are broadly stable with respect to electrochemical characterization and solvent environment (**SI, Figure S5**). For completeness, we note that SAMs formed from an ostensibly pure **CoSS** sample prepared from $Co(OAc)_2 \cdot 4H_2O$ (**SI**, method A; not subjected to chromatographic purification) often exhibited an unusual irreversible redox feature in surface voltammograms that disappeared after ~50 potential cycles (**SI, Figure S4c**; E_{pa} ~ 1-1.2 V). While the origin of this feature remains unclear, it is practically undetectable for **CoSS** SAMs prepared from $CoCl_2 \cdot 6H_2O$ (**SI**, method B; subjected to a chromatographic purification step) and is typically not observed for SAMs formed from **CoSH**, **FeSS**, or **ZnSS**. Equilibrium cyclic voltammograms for SAMs comprising **CoSS** are presented unless otherwise stated. The saturation surface coverages ($\mathbf{\Gamma}$ ~ 34-52 pmol/cm^2), and full width half maximum for surface voltametric peaks (E_{FWHM} ~ 180-230 mV) determined for the **MSS** (M = Fe, Co) SAMs studied here are consistent with reported values for other SAMs comprising charged polypyridyl complexes (**SI, Table S11**).[3,7,45] It has been suggested that the positive shift in the $M^{2+/3+}$ redox potential upon surface binding, lower $\mathbf{\Gamma}$ than predicted for a close-packed monolayer, and greater E_{FWHM} than the 90 mV expected for non-interacting sites is due to repulsive intermolecular interactions within the adsorbed charged layer.[45]

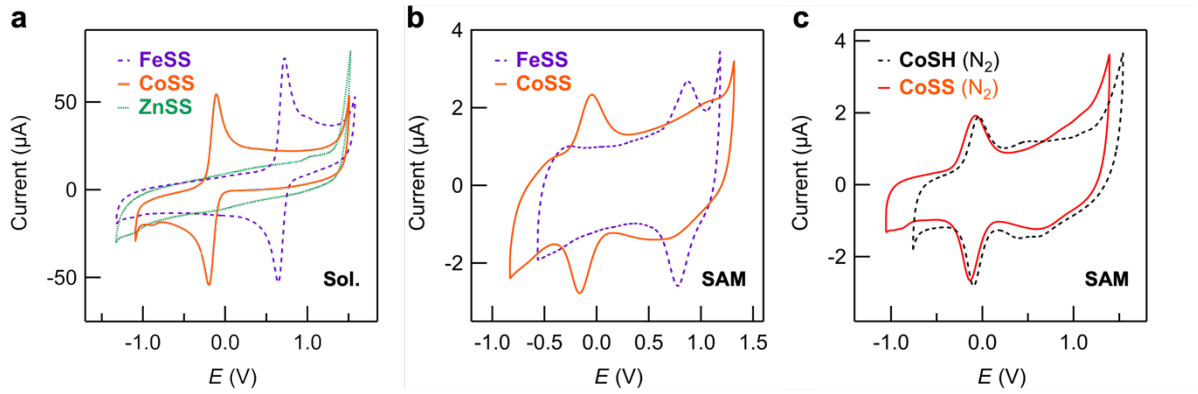

Figure 4. (a) Overlaid solution cyclic voltammograms for **MSS** where M = Fe (purple dashed), Co (orange solid), Zn (green dotted), reproduced from **Figure 3a-c** for convenience. Here the potential window is maintained above −1.4 V vs. the FcH/[FcH]$^+$ redox couple to avoid irreversible reduction of the disulfide group. **(b)** Overlaid representative surface cyclic voltammograms for **FeSS** and **CoSS** SAMs on gold measured over a potential window similar to that used in (a). For each SAM a single redox feature is observed close to the potential of the corresponding $M^{2+/3+}$ couple measured in solution, indicating that the complex is attached to the surface. **(c)** Overlaid cyclic voltammograms obtained for **CoSH** (black dashed) and **CoSS** (orange solid) SAMs prepared under a nitrogen atmosphere in a glovebox. Redox features exhibit similar peak intensities and widths (taking into account electrode-electrode variation) indicating that SAMs of comparable structure and composition are formed from –SH and –SSMe functionalized precursors.

CONCLUSION

In this work we have demonstrated that metal bis(terpyridine) complexes comprising directly connected -SSMe groups are stable in aerated solution, and with respect to electrochemical potentials as low as ~−1.4 V vs. FcH/[FcH]$^+$. We further show that these **MSS** complexes can be used to form SAMs with comparable electrochemical properties to those formed from **CoSH**. It is anticipated that this unconventional protecting group strategy may also prove useful for the installation and utility of stable surface-binding sulfur groups on other compounds, particularly those comprising counterions or prone to decomposition in basic media. We find that **CoSH** is air sensitive in solution, and caution that it must be handled and studied with care to avoid complications arising from its rapid decomposition. Taken together, this work provides a firm basis for subsequent studies focused on single- and multi-component functionalization of metal surfaces using **MSS** precursors, or chemisorbed gold-sulfur linked **MSS** single-molecule junctions.

ASSOCIATED CONTENT

Electronic Supplementary Information (ESI) available: Additional experimental details, synthetic, crystallographic, and electrochemical data, ^{1}H and $^{13}C\{^{1}H\}$ NMR spectra for all new compounds.

AUTHOR INFORMATION

Corresponding Author

Michael S. Inkpen – Email: inkpen@usc.edu

Notes

The authors declare no competing financial interest.

ACKNOWLEDGEMENTS

Acknowledgement is made to the donors of the American Chemical Society Petroleum Research Fund (62751-DNI5), and University of Southern California (USC) startup funds, for support of this research. We thank Nils Rotthowe for useful discussions, and are grateful to the NSF (DBI-0821671, CHE-0840366, CHE-1048807, CHE-2018740) and the NIH (S10 RR25432) for analytical instrumentation.

REFERENCES

1. Park, J., Pasupathy, A. N., Goldsmith, J. I., Chang, C., Yaish, Y., Petta, J. R., Rinkoski, M., Sethna, J. P., Abruña, H. D., McEuen, P. L. & Ralph, D. C. Coulomb blockade and the Kondo effect in single-atom transistors. *Nature* **417**, 722–725 (2002).
2. Parks, J. J., Champagne, A. R., Costi, T. A., Shum, W. W., Pasupathy, A. N., Neuscamman, E., Flores-Torres, S., Cornaglia, P. S., Aligia, A. A., Balseiro, C. A., Chan, G. K. L., Abruña, H. D. & Ralph, D. C. Mechanical control of Spin States in Spin-1 Molecules and the Underscreened Kondo Effect. *Science* **328**, 1370–1373 (2010).
3. Gang, T., Yilmaz, M. D., Ataç, D., Bose, S. K., Strambini, E., Velders, A. H., De Jong, M. P., Huskens, J. & Van Der Wiel, W. G. Tunable doping of a metal with molecular spins. *Nature Nanotechnol.* **7**, 232–236 (2012).
4. Seo, K., Konchenko, A. V., Lee, J., Gyeong, S. B. & Lee, H. Molecular conductance switch-on of single ruthenium complex molecules. *J. Am. Chem. Soc.* **130**, 2553–2559 (2008).
5. Baisch, B., Raffa, D., Jung, U., Magnussen, O. M., Nicolas, C., Lacour, J., Kubitschke, J. & Herges, R. Mounting freestanding molecular functions onto surfaces: The

platform approach. *J. Am. Chem. Soc.* **131**, 442–443 (2009).

6. Dong, T.-Y., Huang, C., Chen, C.-P. & Lin, M.-C. Molecular self-assembled monolayers of ruthenium(II)-terpyridine dithiol complex on gold electrode and nanoparticles. *J. Organomet. Chem.* **692**, 5147–5155 (2007).
7. Campagnoli, E., Hjelm, J., Milios, C. J., Sjodin, M., Pikramenou, Z. & Forster, R. J. Adsorption dynamics and interfacial properties of thiol-based cobalt terpyridine monolayers. *Electrochim. Acta* **52**, 6692–6699 (2007).
8. Murphy, F. A., Suarez, S., Figgemeier, E., Schofield, E. R. & Draper, S. M. Robust self-assembled monolayers of Ru^{II} and Os^{II} polypyridines on gold surfaces: Exploring new potentials. *Chem. Eur. J.* **15**, 5740–5748 (2009).
9. Lee, J., Chang, H., Kim, S., Bang, G. S. & Lee, H. Molecular monolayer nonvolatile memory with tunable molecules. *Angew. Chem. Int. Ed.* **48**, 8501–8504 (2009).
10. Nováková Lachmanová, Š., Vavrek, F., Sebechlebská, T., Kolivoška, V., Valášek, M. & Hromadová, M. Charge transfer in self-assembled monolayers of molecular conductors containing tripodal anchor and terpyridine-metal redox switching element. *Electrochim. Acta* **384**, (2021).
11. Liatard, S., Chauvin, J., Balestro, F., Jouvenot, D., Loiseau, F. & Deronzier, A. An Original Electrochemical Method for Assembling Multilayers of Terpyridine-Based Metallic Complexes on a Gold Surface. *Langmuir* **28**, 10916–10924 (2012).
12. Nerngchamnong, N., Thompson, D., Cao, L., Yuan, L., Jiang, L., Roemer, M. & Nijhuis, C. A. Nonideal Electrochemical Behavior of Ferrocenyl–Alkanethiolate SAMs Maps the Microenvironment of the Redox Unit. *J. Phys. Chem. C* **119**, 21978–21991 (2015).
13. Maskus, M. & Abruña, H. D. Synthesis and Characterization of Redox-Active Metal Complexes Sequentially Self-Assembled onto Gold Electrodes via a New Thiol−Terpyridine Ligand. *Langmuir* **12**, 4455–4462 (1996).
14. Tuccitto, N., Ferri, V., Cavazzini, M., Quici, S., Zhavnerko, G., Licciardello, A. & Rampi, M. A. Highly conductive ∼40-nm-long molecular wires assembled by stepwise incorporation of metal centres. *Nature Mater.* **8**, 41 (2008).
15. Sakamoto, R., Wu, K.-H., Matsuoka, R., Maeda, H. & Nishihara, H. π-Conjugated bis(terpyridine)metal complex molecular wires. *Chem. Soc. Rev.* **44**, 7698–7714 (2015).
16. Tang, J., Wang, Y., Klare, J. E., Tulevski, G. S., Wind, S. J. & Nuckolls, C. Encoding molecular-wire formation within nanoscale sockets. *Angew. Chem. Int. Ed.* **46**, 3892–

3895 (2007).

17. Sullivan, T. P. & Huck, W. T. S. Reactions on Monolayers: Organic Synthesis in Two Dimensions. *European J. Org. Chem.* **2003**, 17–29 (2003).
18. Poisson, J., Geoffrey, H. L., Ebralidze, I. I., Laschuk, N. O., Allan, J. T. S., Deckert, A., Easton, E. B. & Zenkina, O. V. Layer-by-Layer Assemblies of Coordinative Surface-Confined Electroactive Multilayers: Zigzag vs Orthogonal Molecular Wires with Linear vs Molecular Sponge Type of Growth. *J. Phys. Chem. C* **122**, 3419–3427 (2018).
19. Inkpen, M. S., Leroux, Y. R., Hapiot, P., Campos, L. M. & Venkataraman, L. Reversible on-surface wiring of resistive circuits. *Chem. Sci.* **8**, 4340–4346 (2017).
20. Van Der Geer, E. P. L., Van Koten, G., Klein Gebbink, R. J. M. & Hessen, B. A [4Fe-4S] cluster dimer bridged by bis(2,2′:6′,2″- terpyridine-4′-thiolato)iron(II). *Inorg. Chem.* **47**, 2849–2857 (2008).
21. Silva, M. J. J. P., Bertoncello, P., Daskalakis, N. N., Spencer, N., Kariuki, B. M., Unwin, P. R. & Pikramenou, Z. Surface-active mononuclear and dinuclear Ru(II) complexes based on thio-substituted terpyridines bearing cyclodextrin recognition units. *Supramol. Chem.* **19**, 115–127 (2007).
22. Kuehnel, M. F., Orchard, K. L., Dalle, K. E. & Reisner, E. Selective Photocatalytic CO_2 Reduction in Water through Anchoring of a Molecular Ni Catalyst on CdS Nanocrystals. *J. Am. Chem. Soc.* **139**, 7217–7223 (2017).
23. Wen, H.-M., Zhang, D.-B., Zhang, L.-Y., Shi, L.-X. & Chen, Z.-N. Efficient Synthetic Approaches To Access Ruthenium(II) Complexes with 2-(Trimethylsilyl)ethyl- or Acetyl-Protected Terpyridine–Thiols. *Eur. J. Inorg. Chem.* **2011**, 1784–1791 (2011).
24. Bain, C. D., Biebuyck, H. A. & Whitesides, G. M. Comparison of self-assembled monolayers on gold: coadsorption of thiols and disulfides. *Langmuir* **5**, 723–727 (1989).
25. Inkpen, M. S., Liu, Z., Li, H., Campos, L. M., Neaton, J. B. & Venkataraman, L. Non-chemisorbed gold–sulfur binding prevails in self-assembled monolayers. *Nature. Chem.* **11**, 351–358 (2019).
26. Horikoshi, R. & Mochida, T. Metal complexes of 4,4′-dipyridyldisulfide-structural diversity derived from a twisted ligand with axial chirality. *Coord. Chem. Rev.* **250**, 2595–2609 (2006).
27. Constable, E. C., Hermann, B. A., Housecroft, C. E., Neuburger, M., Schaffner, S. & Scherer, L. J. 2,2′:6,2″-Terpyridine-4′(1′H)-thione: A missing link in

metallosupramolecular chemistry. *New J. Chem.* **29**, 1475–1481 (2005).

28. Heister, K., Allara, D. L., Bahnck, K., Frey, S., Zharnikov, M. & Grunze, M. Deviations from 1:1 compositions in self-assembled monolayers formed from adsorption of asymmetric dialkyl disulfides on gold. *Langmuir* **15**, 5440–5443 (1999).
29. Bain, C. D. & Whitesides, G. M. Formation of monolayers by the coadsorption of thiols on gold: Variation in the length of the alkyl chain. *J. Am. Chem. Soc.* **111**, 7164–7175 (1989).
30. Porter, M. D., Bright, T. B., Allara, D. L. & Chidsey, C. E. D. Spontaneously organized molecular assemblies. 4. Structural characterization of n-alkyl thiol monolayers on gold by optical ellipsometry, infrared spectroscopy, and electrochemistry. *J. Am. Chem. Soc.* **109**, 3559–3568 (1987).
31. Kitson, T. M. & Loomes, K. M. Synthesis of methyl 2- and 4-pyridyl disulfide from 2- and 4-thiopyridone and methyl methanethiosulfonate. *Anal. Biochem.* **146**, 429–430 (1985).
32. Harzmann, G. D., Neuburger, M. & Mayor, M. 4,4″-Disubstituted Terpyridines and their Homoleptic Fe^{II} Complexes. *Eur. J. Inorg. Chem.* **2013**, 3334–3347 (2013).
33. Constable, E. C., Housecroft, C. E., Kulke, T., Lazzarini, C., Schofield, E. R. & Zimmermann, Y. Redistribution of terpy ligands—approaches to new dynamic combinatorial libraries. *J. Chem. Soc. Dalt. Trans.* 2864–2871 (2001).
34. Gryko, D. T., Clausen, C., Roth, K. M., Dontha, N., Bocian, D. F., Kuhr, W. G. & Lindsey, J. S. Synthesis of 'Porphyrin-linker-thiol' molecules with diverse linkers for studies of molecular-based information storage. *J. Org. Chem.* **65**, 7345–7355 (2000).
35. Chow, H. S., Constable, E. C., Housecroft, C. E., Kulicke, K. J. & Tao, Y. When electron exchange is chemical exchange–assignment of ^{1}H NMR spectra of paramagnetic cobalt(II)-2,2′:6′,2″-terpyridine complexes. *Dalton Trans.* 236–237 (2005).
36. Miao, Z., Quainoo, T., Czyszczon-Burton, T. M., Rotthowe, N., Parr, J. M., Liu, Z. & Inkpen, M. S. Charge transport across dynamic covalent chemical bridges. *Nano Lett.* **22**, 8331–8338 (2022).
37. Borsari, M., Cannio, M. & Gavioli, G. Electrochemical behavior of diphenyl disulfide and thiophenol on glassy carbon and gold electrodes in aprotic media. *Electroanalysis* **15**, 1192–1197 (2003).
38. Widrig, C. A., Chung, C. & Porter, M. D. The electrochemical desorption of n-alkanethiol monolayers from polycrystalline Au and Ag electrodes. *J. Electroanal.*

Chem. Interfacial Electrochem. **310**, 335–359 (1991).

39. Maran, F., Wayner, D. D. M. & Workentin, M. S. *Kinetics and mechanism of the dissociative reduction of C−X and X−X bonds (X = O, S)*. *Advances in Physical Organic Chemistry* vol. 36 (2001).
40. Hall, G. B., Kottani, R., Felton, G. A. N., Yamamoto, T., Evans, D. H., Glass, R. S. & Lichtenberger, D. L. Intramolecular electron transfer in bipyridinium disulfides. *J. Am. Chem. Soc.* **136**, 4012–4018 (2014).
41. Hansch, C., Leo, A. & Taft, R. W. A survey of Hammett substituent constants and resonance and field parameters. *Chem. Rev.* **91**, 165–195 (1991).
42. Lam, K. & Geiger, W. E. Anodic Oxidation of Disulfides: Detection and Reactions of Disulfide Radical Cations. *J. Org. Chem.* **78**, 8020–8027 (2013).
43. Bewick, A., Coe, D. E., Libert, M. & Mellor, J. M. Mechanism of anodic acetamidosulphenylation and acetamidoselenation of alkenes. *J. Electroanal. Chem.* **144**, 235–250 (1983).
44. Bard, A. J. & Faulkner, L. Y. *Electrochemical Methods*. (Wiley, 2004).
45. Figgemeier, E., Merz, L., Hermann, B. A., Zimmermann, Y. C., Housecroft, C. E., Gu, H.-J. & Constable, E. C. Self-Assembled Monolayers of Ruthenium and Osmium Bis-Terpyridine Complexes Insights of the Structure and Interaction Energies by Combining Scanning Tunneling Microscopy and Electrochemistry. *J. Phys. Chem. B* **107**, 1157–1162 (2003).

For Table of Contents Only

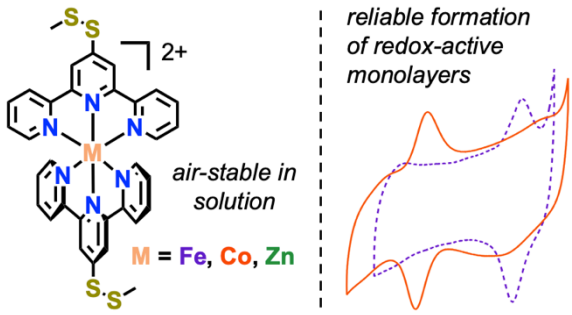

A new ligand comprising directly-connected disulfide-based anchors provides access to air-stable metal bis(terpyridine) complexes for the functionalization of metal surfaces.

Supplementary Information

Methyldisulfide groups enable the direct connection of air-stable metal bis(terpyridine) complexes to gold surfaces

Christina D.M. Trang, Thomas Saal, and Michael S. Inkpen*

Department of Chemistry, University of Southern California, Los Angeles, California 90089, United States

E-mail: inkpen@usc.edu

Contents

1. General Information

Synthetic Methods

All manipulations were carried out in oven-dried glassware under a nitrogen atmosphere using standard Schlenk line techniques, or inside of an OMNI-Lab 4-port glovebox (Vacuum Atmospheres Company, Hawthorne, CA, USA. No special precautions were taken to exclude air or moisture during workup unless otherwise stated. Dichloromethane was sparged with nitrogen and dried using a two-column solvent purification system packed with alumina (Pure Process Technologies, Nashua, NH, USA). *N*,*N*-Dimethylformamide (DMF) was purified by vacuum distillation, dried over 3Å molecular sieves, and stored under nitrogen. Other reaction solvents (sparged with nitrogen prior to use) and chemical regents were commercially available and used without further purification. 18.2 MΩ water was generated using an Arium® Mini Plus UV ultrapure water system (Sartorius AG, Goettingen, Germany). Deuterated solvents were purchased from Cambridge Isotope Laboratories, Inc., Cambridge Isotope Laboratories, Tewksbury, MA USA. Flash chromatography was performed using a Pure C-850 FlashPrep chromatography system and FlashPure EcoFlex flash cartridges (neutral alumina, irregular 50-75 μm particle size, 50-70 Å pore size; BUCHI Corporation, New Castle, DE, USA), or by hand using neutral alumina adjusted to Brockmann activity V (15% H_2O; Acros Organics, 50-200 μm particle size, 60 Å pore size). Suspensions were separated using a VanGuard V6500 centrifuge (Hamilton Bell, Montvale, NJ, USA).

^{1}H and ^{13}C{^{1}H} NMR spectra were recorded at room temperature on Varian VNMRS 500 (500 MHz), VNMRS 600 (600 MHz), or Mercury 400 (400 MHz) NMR spectrometers, unless otherwise stated. ^{1}H NMR data recorded in $CDCl_3$, MeCN-d_3, DMSO-d_6, and acetone-d_6 is referenced to residual internal C*H*Cl_3 (δ 7.26), C*H*D_2CN (δ 1.94), (C*H*D_2)(CD_3)SO (δ 2.50), and (C*H*D_2)(CD_3)CO (δ 2.05) solvent signals.[1] ^{13}C{^{1}H} NMR data recorded in $CDCl_3$ and MeCN-d_3 is referenced to internal *C*DCl_3 (δ 77.16) and *C*D_3CN (δ 1.32).[1] ^{1}H and ^{13}C{^{1}H} resonances were assigned where possible for new compounds using 2D correlation spectroscopy experiments. Mass spectrometry analyses were performed on a Waters Synapt G2-Si at the Mass Spectrometry Lab, University of Illinois Urbana-Champaign. Microanalyses were carried out using a Control Equipment Corp. CEC 440HA Elemental Analyzer at the Marine Science Institute, University of California Santa Barbara (found values are the average of two runs).

X-Ray Crystallography

*For **tpySSMe**, **FeSS**, **CoSS**:* X-ray intensity data were collected at 100 K on a Bruker APEX DUO 3-circle platform diffractometer, equipped with an APEX II CCD detector, using MoKα radiation (λ = 0.71073 Å, TRIUMPH curved-crystal monochromator) from a fine-focus tube. The structures were solved by intrinsic phasing and refined on F^2 using the Bruker APEX3 Software Package and ShelXle.[2–5] *For **ZnSS**:* X-ray intensity data were collected on a Rigaku XtaLAB Synergy, Dualflex, equipped with a HyPix-6000HE pixel array detector, using CuKα radiation (λ = 1.54184 Å) from microfocus sealed tube. The structure was solved using dual methods and refined on F^2 using ShelXle.[3–6] All non-hydrogen atoms were refined anisotropically. Further crystallographic details can be obtained from the Cambridge Crystallographic Data Centre (CCDC, 12 Union Road, Cambridge, CB2 1EZ, UK (Fax: (+44) 1223–336–033; e-mail: deposit@ccdc.cam.ac.uk) on quoting the deposition no. CCDC 2220466-2220469.

Electrochemical Methods

Electrochemical measurements were performed under an argon atmosphere using a CHI760E bipotentiostat (CH Instruments, Austin, TX, USA) with argon or nitrogen-sparged 0.1 M tetrabutylammonium hexafluorophosphate (NBu_4PF_6) MeCN or CH_2Cl_2 solutions (using non-anhydrous solvents). Unless otherwise stated, solution voltammograms were obtained in MeCN (scan rate = 0.1 V s^{-1}), and surface voltammograms in CH_2Cl_2 (scan rate = 1 V s^{-1}). Plotted voltammograms are not corrected for iR_s unless otherwise stated. Solution studies employed glassy carbon disc working electrodes (Ø = 3 mm, CH Instruments), mechanically polished using an alumina slurry prior to use. Pt wire reference and counter electrodes were cleaned by annealing in an oxyhydrogen flame. Analyte solutions were between 0.1-1 mM. Potentials are reported relative to $[Cp_2Fe]^+/[Cp_2Fe]$ (unless otherwise stated), measured against internal Cp_2Fe or Cp^*_2Fe references as appropriate.

Gold disk electrodes (⌀ = 2 mm; CH Instruments) used for SAM studies were first cleaned by mechanical polishing using an alumina slurry (0.05 μm). After thorough rinsing with 18.2 MΩ water, they were agitated in piranha solution (conc. H_2SO_4−30% H_2O_2, 3:1 w/w) for 1 min, rinsed with 18.2 MΩ water and ethanol, then immersed in ethanol for ≥20 min.[7] After cleaning, electrodes were immediately immersed in 1 mM solutions of analyte in MeCN for ≥18 h to form SAMs,

unless otherwise stated. Prior to electrochemical measurements, the electrodes were removed from the SAM formation solutions and washed thoroughly with MeCN then the solvent used for electrochemical measurements (e.g., CH_2Cl_2).

SAMs of **CoSS** and **CoSH** formed under an inert nitrogen atmosphere were prepared inside of an OMNI-Lab 4-port glovebox (Vacuum Atmospheres Company, Hawthorne, CA, USA). Clean gold disc electrodes were pumped into the glovebox, then immersed for 18-24 h in 1 mM **CoSS** or **CoSH** solutions in MeCN (dried over 3Å sieves, sparged with nitrogen). After emersion, the electrodes were washed thoroughly with MeCN and CH_2Cl_2 (dried over 3Å sieves, sparged with nitrogen) then integrated into a custom air-tight three electrode cell comprising Pt counter and reference electrodes. A solution of 0.1 M NBu_4PF_6 in CH_2Cl_2 was added, then the sealed cell was removed from the glovebox to perform electrochemical measurements.

The average real surface area of the gold electrodes used in these experiments was determined by measuring cyclic voltammograms between −0.2 and 1.6 V versus Ag/AgCl in aqueous 0.1 M H_2SO_4. The area was calculated from the charge obtained for the gold reduction peak (first cycle, using a scan rate of 5 V s^{-1}) divided by the reference charge of 390 μC cm^{-2} for reduction of an oxide monolayer on polycrystalline gold.[8,9] From two sets of three electrodes (prepared and measured on different days) we obtained a real surface area of 0.073 ± 0.012 (1 s.d.) cm^2, corresponding to a roughness factor of ~2.3.

Gold-on-glass substrates for selected electrochemical studies were prepared by evaporation of 5 nm chromium (Angstrom Engineering Inc., ON, Canada) then 200 nm gold (99.9985%, Alfa Aesar) onto <1 cm^2 glass substrates cut from 3" × 1" × 1 mm microscope slides (Premium Plain VWR Micro Slides, VWR International, LLC, USA), using a COVAP Physical Vapor Deposition System (Angstrom Engineering Inc., ON, Canada) applied exclusively for metal evaporation. Prior to metal evaporation, glass substrates were cleaned by boiling in a 20% nitric acid bath for 10 minutes, rinsed with 18.2 MΩ water, then dried and stored at 120 °C. Gold-on-glass substrates were used without further processing on the same day as metal evaporation.

2. Synthetic Details

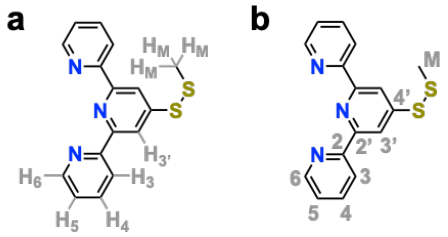

Figure S1. NMR labelling scheme for terpyridine **(a)** ^{1}H and **(b)** ^{13}C{^{1}H} resonances. Resonances for **tpySH** and **CoSH** follow the same scheme but omit H_M and C_M.

*4'-Methyldisulfide-2,2':6,2''-terpyridine (**tpySSMe**)*

This synthetic procedure was adapted from literature methods.[10,11] Anhydrous DMF (72 mL) was added to 4'-chloro-2,2':6',2"-terpyridine (0.993 g, 3.71 mmol) and NaSH · xH_2O (≥60%; 5.369 g, ≥57.5 mmol) in a 200 mL Schlenk flask equipped with a stir bar and condenser. The yellow mixture was heated to reflux for 4 h with stirring, cooled to room temperature, then filtered through a glass fritted filter. Solvent was removed by rotary evaporation and the yellow residue re-dissolved in water (50 mL) whereby an aqueous 1 M HCl solution was added dropwise to precipitate the product from solution. The suspended solid was isolated by filtration, washed with water, then dried under vacuum to yield 2,2':6',2"-terpyridine-4'-thiol (**tpySH**) as a bright yellow solid (0.905 g, 92%). Spectroscopic data was generally consistent with previous reports.[10] ^{1}H NMR (DMSO-d_6, 400 MHz): ***δ*** (ppm) 7.63 (m, 2H), 8.05 (td, 2H, J = 1.7 and 7.9 Hz), 8.14 (br s, 2H), 8.44 (d, 2H, J = 8.0 Hz), 8.85 (d, 2H, J = 4.7 Hz), −SH/−NH proton not observed. HR-MS (ESI+) *m/z*: 266.0751 ($[M+H]^+$ calc. for $C_{15}H_{12}N_3S$ 266.0752).

Water (4 mL) was added to **tpySH** (0.994 g, 3.75 mmol) and NaOH (0.154 g, 3.85 mmol) in a Schlenk flask equipped with a stir bar. After full dissolution of solid materials, S-methyl methanethiosulfonate (0.35 mL, 3.7 mmol) was added dropwise via syringe with stirring, forming a light-yellow suspension. After stirring at room temperature for 2 h, the opaque yellow mixture was extracted with CH_2Cl_2 (3 × 10 mL), dried with $MgSO_4$, and filtered. Solvent was removed under vacuum, whereby the crude product (yellow oil) was adsorbed onto Celite and purified by column chromatography (alumina V; hexanes/ethyl acetate [1:0 → 9:1 v/v]). Evaporation of selected fractions provided **tpySSMe** as a white solid (0.987 g, 86% yield). Single crystals suitable for X-ray diffraction were grown from vapor diffusion of pentane into a $CHCl_3$ solution. ^{1}H NMR

($CDCl_3$, 600 MHz): ***δ*** (ppm) 2.51 (s, 3H, H_M), 7.30 (m, 2H, H_5), 7.81 (td, 2H, J = 1.6 and 7.6 Hz, H_4), 8.57 (d, 2H, J = 7.9 Hz, H_3), 8.61 (s, 2H, $H_{3'}$), 8.69 (d, 2H, J = 4.68 Hz, H_6). ^{1}H NMR (MeCN-d_3, 400 MHz): ***δ*** (ppm) 2.55 (s, 3H), 7.44 (m, 2H), 7.95 (td, 2H, J = 1.7 and 7.9 Hz), 8.62 (s, 2H), 8.64 (d, 2H, J = 8.0 Hz), 8.70 (d, 2H, J = 4.7 Hz). ^{13}C{^{1}H} NMR ($CDCl_3$, 150 MHz): ***δ*** (ppm) 23.06 (C_M), 117.22 ($C_{3'}$), 121.46 (C_3), 124.00 (C_5), 136.85 (C_4), 149.21 (C_6), 150.86 ($C_{4'}$), 155.57 (C_2), 155.72 ($C_{2'}$). HR-MS (ESI+) *m/z*: 312.0626 ($[M+H]^+$ calc. for $C_{16}H_{14}N_3S_2$: 312.0629). Anal. Calc. for $C_{16}H_{13}N_3S_2$: C, 61.71; H, 4.21; N, 13.49%. Found: C, 61.61; H, 4.38; N, 13.14%.

*[Fe(**tpySSMe**)$_2$][PF$_6$]$_2$ (**FeSS**)*

This synthetic procedure was adapted from literature methods.[12] Methanol (7.5 mL) was added to **tpySSMe** (0.115 g, 0.370 mmol) and $FeCl_2 \cdot 4H_2O$ (0.038 g, 0.19 mmol) in a Schlenk flask equipped with a stir bar. The resulting dark purple solution was stirred for 1 h, then NH_4PF_6 (0.300 g, 1.85 mmol) in H_2O (1 mL) was added to precipitate the PF_6^- salt. After stirring for 10 min the suspension was centrifuged, the supernatant discarded, and the precipitate washed with additional H_2O to remove residual NH_4PF_6. Remaining solid material was dissolved in a minimum quantity of MeCN (~2 mL) then reprecipitated using excess diethyl ether (~10 mL). The suspension was again separated by centrifugation, washing the precipitate with additional diethyl ether to remove residual solvents and uncoordinated ligand. The isolated solid material was dried under vacuum to provide **FeSS** as a deep purple powder (0.165 g, 92% yield). Single crystals suitable for X-ray diffraction were grown by vapor diffusion of diethyl ether into a MeCN solution. ^{1}H NMR (MeCN-d_3, 500 MHz): ***δ*** (ppm) 2.83 (s, 6H, H_M), 7.09 (m, 4H, H_5), 7.16 (d, 4H, J = 5.6 Hz, H_6), 7.89 (td, 4H, J = 1.3 and 7.8 Hz, H_4), 8.53 (d, 4H, J = 7.9 Hz, H_3), 9.02 (s, 4 H, $H_{3'}$). ^{13}C{^{1}H} NMR (MeCN-d_3, 125 MHz): ***δ*** (ppm) 23.55 (C_M), 120.61 ($C_{3'}$), 125.05 (C_3), 128.45 (C_5), 139.69 (C_4), 153.85 ($C_{4'}$), 154.32 (C_6), 158.44 (C_2), 160.60 ($C_{2'}$). HR-MS (ESI+) *m/z*: 339.0225 ($[M]^{2+}$ calc. for $C_{32}H_{26}FeN_6S_4$: 339.0226). Anal. Calc. for $C_{32}H_{26}F_{12}FeN_6P_2S_4$: C, 39.68; H, 2.71; N, 8.68%. Found: C, 39.71; H, 2.64; N, 9.11%.

*[Co(**tpySSMe**)$_2$][PF$_6$]$_2$ (**CoSS**)*

These representative synthetic procedures were adapted from literature methods.[13,14] <u>*Method A:*</u> A mixture of MeOH (10 mL), $Co(OAc)_2 \cdot 4H_2O$ (0.064 g, 0.257 mmol), and **tpySSMe** (0.157 g, 0.504 mmol) was stirred at room temperature for 2 h. The resulting orange-brown solution was reduced in volume by rotary evaporation, whereby a solution of KPF_6 (0.429 g, 2.33 mmol) in water (5

mL) was added to precipitate the PF_6^- salt. The suspended solid was purified by centrifugation following the method described above for **FeSS**, providing **CoSS** as a dark orange powder (0.172 g, 70% yield). Single crystals suitable for X-ray diffraction were grown by vapor diffusion of diethyl ether into a MeCN solution. ^{1}H NMR (MeCN-d_3, 400 MHz): ***δ*** (ppm) 6.17 (s, 6H), 8.32 (s, 4H), 34.38 (s, 4H), 54.46 (s, 4H), 61.16 (s, 4H), 102.44 (br s, 4H). HR-MS (ESI+) *m/z*: 340.5213 ($[M]^{2+}$ calc. for $C_{32}H_{26}CoN_6S_4$: 340.5217). Anal. Calc. for $C_{32}H_{16}CoF_{12}N_6P_2S_4$: C, 39.55; H, 2.70; N, 8.65%. Found: C, 39.16; H, 2.60; N, 8.42%.

Method B: A mixture of $CoCl_2 \cdot 6H_2O$ (0.059 g, 0.248 mmol) and **tpySSMe** (0.158 g, 0.509 mmol) in MeOH (10 mL) was stirred at room temperature for 1 h, providing an orange-brown solution. Solvent was removed by rotary evaporation to yield a dark red-orange solid. The crude product was purified via column chromatography (alumina V, sample loaded in a minimum amount of solvent), collecting the dark red fraction that elutes with 10% MeOH in CH_2Cl_2. The solid residue obtained after solvent removal by rotary evaporation was re-dissolved in MeOH (5 mL), whereby a solution of KPF_6 (0.470 g, 2.55 mmol) in water (20 mL) was added to precipitate the PF_6^- salt. The suspended solid was purified by centrifugation following the method described above for **FeSS**, providing **CoSS** as a dark orange powder (0.101 g, 42% yield). Spectroscopic data matched that for samples prepared via *Method A*.

*[Co(**tpySSMe**)$_2$][PF$_6$]$_3$ (**CoSS^{3+}**)*

A solution of $AgPF_6$ in acetone (0.52 mL, 0.28 M, 0.15 mmol; stored in the absence of light) was added to an orange solution of **CoSS** (0.073 g, 0.075 mmol) in acetone (1 mL), resulting in an immediate colour change to dark green/brown. The silver precipitate was removed by syringe filtration (PTFE membrane, 0.2 μm pore size) to provide a yellow-orange solution. Removal of solvent under vacuum yielded **CoSS^{3+}** as a yellow-orange solid (0.082 g, quant. yield). ^{1}H NMR (MeCN-d_3, 400 MHz): ***δ*** (ppm) 2.83 (s, 6H, H_M), 7.36 (dd, 4H, J = 0.9 and 5.8 Hz, H_6), 7.45 (m, 4H, H_5), 8.23 (td, 4H, J = 1.4 and 7.9 Hz, H_4), 8.63 (dd, 4H, J = 1.1 and 8.0 Hz, H_3), 9.07 (s, 4H, $H_{3'}$). ^{13}C{^{1}H} NMR (MeCN-d_3, 150 MHz): ***δ*** (ppm) 23.44 (C_M), 123.96 ($C_{3'}$), 128.38 (C_3), 132.02 (C_5), 144.04 (C_4), 153.55 (C_6), 155.85 ($C_{2'}$), 156.62 (C_2), 164.76 ($C_{4'}$). HR-MS (ESI+) *m/z*: 227.0140 ($[M]^{3+}$ calc. for $C_{32}H_{26}CoN_6S_4$: 227.0145).

*[Co(**tpySH**)$_2$][PF$_6$]$_2$ (**CoSH**)*

This procedure was adapted from the one used to prepare **CoSS**, with the strict exclusion of air during both reaction and workup. MeOH (18 mL) was added to a Schlenk flask containing $CoCl_2 \cdot 6H_2O$ (0.101 g, 0.424 mmol) and **tpySH** (0.243 g, 0.916 mmol), resulting in a dark orange solution that was stirred at room temperature for 1 h. The solvent was reduced to ~1/4 of its volume under vacuum, whereby KPF_6 (0.842 g, 4.57 mmol) in H_2O (25 mL) was added to precipitate the PF_6^- salt. The orange precipitate was cannula filtered then washed with degassed H_2O (2 × 10 mL). Solid material was dissolved in MeCN (~5 mL) then precipitated by addition of ether (~25 mL). This suspension was cannula filtered and washed with ether (2 × 10 mL) then dried under vacuum overnight. The flask was transferred to a glovebox whereby **CoSH** was isolated as a brown-orange solid (0.186 g, 50%). ^{1}H NMR (MeCN-d_3, 500 MHz): ***δ*** (ppm) 7.64 (s, 4H), 11.33 (s, 2H), 34.78 (s, 4H), 62.23 (s, 4H), 64.61 (s, 4H), 106.65 (s, 4H). HR-MS (ESI+) m/z: 294.5340 ($[M]^{2+}$ calc. for $C_{30}H_{22}N_6S_2Co$: 294.5340). Anal. Calc. for $C_{32}H_{26}F_{12}N_6P_2S_4Co$ C, 40.97; H, 2.52; N, 9.56%. Found: C, 40.62; H, 2.55; N, 9.45%.

*[Zn(**tpySSMe**)$_2$][PF$_6$]$_2$ (**ZnSS**)*

This synthetic procedure was adapted from literature methods.[15] A solution of $Zn(OAc)_2 \cdot 2H_2O$ (0.043 g, 0.20 mmol) in MeOH (2 mL) was added to a solution of **tpySSMe** (0.123 g, 0.395 mmol) in CH_2Cl_2 (4 mL). The pale-yellow mixture was stirred at room temperature for 20 h, whereby solvent was removed by rotary evaporation. The crude residue was dissolved in water (~5 mL), then excess KPF_6 (0.321 g, 1.74 mmol) was added to precipitate a yellow solid. This precipitate was purified by centrifugation following the method described above for **FeSS**, providing **ZnSS** as an off-white solid (0.072 g, 37% yield). Single crystals suitable for X-ray diffraction were grown by vapor diffusion of diethyl ether into a MeCN solution. ^{1}H NMR (MeCN-d_3, 400 MHz): ***δ*** (ppm) 2.73 (s, 6H, H_M), 7.40 (m, 4H, H_5), 7.82 (d, 4H, J = 5.1 Hz, H_6), 8.15 (t, 4H, J = 8.0 Hz, H_4), 8.60 (d, 4H, J = 8.1 Hz, H_3), 8.83 (s, 4H, $H_{3'}$). ^{13}C{^{1}H} NMR (MeCN-d_3, 150 MHz): ***δ*** (ppm) 23.35 (C_M), 119.99 ($C_{3'}$), 124.27 (C_3), 128.68 (C_5), 142.27 (C_4), 148.41 (C_2), 149.15 (C_6), 150.13 ($C_{2'}$), 160.67 ($C_{4'}$). HR-MS (ESI+) *m/z*: 343.0188 ($[M]^{2+}$ calc. for $C_{32}H_{26}N_6S_4Zn$: 343.0197). Anal. Calc. for $C_{32}H_{26}F_{12}N_6P_2S_4Zn$: C, 39.29; H, 2.68; N, 8.59%. Found: C, 38.91; H, 2.44; N, 8.64%.

3. X-Ray Crystallography

Table S1. Sample and crystal data for **tpySSMe**.

Chemical formula	$C_{16}H_{13}N_3S_2$	
Formula weight	311.41 g/mol	
Temperature	100(2) K	
Wavelength	1.54178 Å	
Crystal size	0.101 x 0.146 x 0.254 mm	
Crystal habit	clear colourless blade	
Crystal system	monoclinic	
Space group	P 1 2_1/c 1	
Unit cell dimensions	a = 8.8399(2) Å	α = 90°
	b = 15.3680(3) Å	β = 96.1950(10)°
	c = 10.8169(2) Å	γ = 90°
Volume	1460.91(5) $Å^3$	
Z	4	
Density (calculated)	1.416 g/cm^3	
Absorption coefficient	3.260 mm^{-1}	
F(000)	648	

Table S2. Data collection and structure refinement for **tpySSMe**.

Diffractometer	Bruker APEX DUO
Radiation source	IμS microsource, CuKα
Theta range for data collection	5.02 to 70.13°
Index ranges	-10<=h<=10, -18<=k<=17, -13<=l<=12
Reflections collected	23417
Independent reflections	2773 [R(int) = 0.0374]
Coverage of independent reflections	99.8%
Absorption correction	multi-scan
Max. and min. transmission	0.753 and 0.618
Structure solution technique	direct methods
Structure solution program	SHELXTL XT 2014/5 (Bruker AXS, 2014)
Refinement method	Full-matrix least-squares on F^2
Refinement program	SHELXTL XL 2014/7 (Bruker AXS, 2014)
Function minimized	$\Sigma\, w(F_o^2 - F_c^2)^2$
Data / restraints / parameters	2773 / 0 / 191
Goodness-of-fit on F^2	1.075
Δ/σ_{max}	0.001
Final R indices	2572 data; I>2σ(I) $R_1 = 0.0289$, $wR_2 = 0.0797$
	all data $R_1 = 0.0313$, $wR_2 = 0.0817$
Weighting scheme	$w=1/[\sigma^2(F_o^2)+(0.0420P)^2+0.8770P]$ where $P=(F_o^2+2F_c^2)/3$
Largest diff. peak and hole	0.366 and -0.366 eÅ^{-3}
R.M.S. deviation from mean	0.049 eÅ^{-3}

Table S3. Sample and crystal data for **FeSS**.

Chemical formula	$C_{34}H_{29}F_{12}FeN_7P_2S_4$	
Formula weight	1009.67 g/mol	
Temperature	100 (2) K	
Wavelength	1.54178 Å	
Crystal size	0.044 x 0.183 x 0.270 mm	
Crystal habit	clear red prism	
Crystal system	monoclinic	
Space group	P 1 2_1 1	
Unit cell dimensions	a = 8.7953(2) Å	α = 90°
	b = 33.8428(8) Å	β = 92.314(2)°
	c = 14.0963(3) Å	γ = 90°
Volume	4192.45(16) $Å^3$	
Z	4	
Density (calculated)	1.600 g/cm^3	
Absorption coefficient	6.322 mm^{-1}	
F(000)	2128	

Table S4. Data collection and structure refinement for **FeSS**.

Diffractometer	Bruker APEX DUO
Radiation source	IμS microsource, CuKα
Theta range for data collection	2.61 to 70.07°
Index ranges	-10<=h<=10, 0<=k<=40, 0<=l<=17
Reflections collected	7951
Independent reflections	7951 [R(int) = 0.1455]
Coverage of independent reflections	98.1%
Absorption correction	multi-scan
Max. and min. transmission	0.753 and 0.527
Structure solution technique	direct methods
Structure solution program	SHELXL 2014/4 (Bruker AXS, 2014)
Refinement method	Full-matrix least-squares on F^2
Refinement program	SHELXL 2014/7 (Bruker AXS, 2014)
Function minimized	$\Sigma\, w(F_o^2 - F_c^2)^2$
Data / restraints / parameters	7951 / 101 / 1118
Goodness-of-fit on F^2	1.037
Δ/σ_{max}	0.010
Final R indices	6858 data; I>2σ(I) $R_1 = 0.0618$, $wR_2 = 0.1342$
	all data $R_1 = 0.0807$, $wR_2 = 0.1416$
Weighting scheme	$w=1/[\sigma^2(F_o^2)+(0.0535P)^2+11.3694P]$ where $P=(F_o^2+2F_c^2)/3$
Absolute structure parameter	0.490(16)
Largest diff. peak and hole	0.540 and -0.453 eÅ^{-3}
R.M.S. deviation from mean	0.101 eÅ^{-3}

Table S5. Sample and crystal data for **CoSS**.

Chemical formula	$C_{38}H_{35}CoF_{12}N_9P_2S_4$	
Formula weight	1094.86 g/mol	
Temperature	100 (2) K	
Wavelength	1.54178 Å	
Crystal size	0.064 x 0.142 x 0.267 mm	
Crystal habit	clear dark purple-red blade-like	
Crystal system	monoclinic	
Space group	P 1 2_1/c 1	
Unit cell dimensions	a = 8.9247 (3) Å	α = 90°
	b = 36.9029(12) Å	β = 93.753(2)°
	c = 13,7769(5) Å	γ = 90°
Volume	4527.7(3) $Å^3$	
Z	4	
Density (calculated)	1.606 g/cm^3	
Absorption coefficient	6.185 mm^{-1}	
F(000)	2220	

Table S6. Data collection and structure refinement for **CoSS**.

Diffractometer	Bruker APEX DUO
Radiation source	IμS microsource, CuKα
Theta range for data collection	2.39 to 69.32°
Index ranges	-10<=h<=10, -42<=k<=44, -16<=l<=16
Reflections collected	48292
Independent reflections	8258 [R(int) = 0.1078]
Coverage of independent reflections	97.3%
Absorption correction	multi-scan
Max. and min. transmission	0.637 and 0.441
Structure solution technique	direct methods
Structure solution program	SHELXL 2014/4 (Bruker AXS, 2014)
Refinement method	Full-matrix least-squares on F^2
Refinement program	SHELXL 2014/7 (Bruker AXS, 2014)
Function minimized	$\Sigma\, w(F_o^2 - F_c^2)^2$
Data / restraints / parameters	8258 / 145 / 613
Goodness-of-fit on F^2	1.163
Δ/σ_{max}	0.003
Final R indices	6858 data; I>2σ(I) $R_1 = 0.0851$, $wR_2 = 0.1886$
	all data $R_1 = 0.1061$, $wR_2 = 0.1973$
Weighting scheme	$w=1/[\sigma^2(F_o^2)+33.7607P]$ where $P=(F_o^2+2F_c^2)/3$
Largest diff. peak and hole	0.573 and -0.573 eÅ^{-3}
R.M.S. deviation from mean	0.108 eÅ^{-3}

Table S7. Sample and crystal data for **ZnSS**.

Chemical formula	$C_{32}H_{26}F_{12}N_6P_2S_4Zn$	
Formula weight	978.14 g/mol	
Temperature	100.00(11) K	
Wavelength	1.54184 Å	
Crystal size	0.19 x 0.11 x 0.04 mm	
Crystal habit	clear pale-yellow plates	
Crystal system	monoclinic	
Space group	P 1 2_1/c 1	
Unit cell dimensions	a = 9.0282(2) Å	α = 90°
	b = 9.5422(2) Å	β = 94.579(2)°
	c = 43.8494(7) Å	γ = 90°
Volume	3765.52(13) $Å^3$	
Z	4	
Density (calculated)	1.725 g/cm^3	
Absorption coefficient	4.657 mm^{-1}	
F(000)	1968	

Table S8. Data collection and structure refinement for **ZnSS**.

Diffractometer	XtaLAB Synergy, Dualflex, HyPix
Radiation source	micro-focus sealed X-ray tube, CuKα
Theta range for data collection	4.046 to 80.165°
Index ranges	-11<=h<=11, -8<=k<=12, -56<=l<=55
Reflections collected	33496
Independent reflections	7704 [R(int) = 0.0956]
Coverage of independent reflections	98.2%
Absorption correction	multi-scan
Max. and min. transmission	1.000 and 0.795
Structure solution technique	dual methods
Structure solution program	SHELXL 2014/5 (Sheldrick, 2014)
Refinement method	Full-matrix least-squares on F^2
Refinement program	SHELXL 2017/1 (Sheldrick, 2015)
Function minimized	$\Sigma\, w(F_o^2 - F_c^2)^2$
Data / restraints / parameters	7704 / 137 / 609
Goodness-of-fit on F^2	1.029
Δ/σ_{max}	0.002
Final R indices	5993 data; I>2σ(I) $R_1 = 0.0734$, $wR_2 = 0.1888$
	all data $R_1 = 0.0925$, $wR_2 = 0.2032$
Weighting scheme	$w=1/[\sigma^2(F_o^2)+(0.1017P)^2+13.4453P]$ where $P=(F_o^2+2F_c^2)/3$
Largest diff. peak and hole	1.683 and -1.064 eÅ^{-3}
R.M.S. deviation from mean	0.114 eÅ^{-3}

4. Electrochemistry

Solution Voltammetry

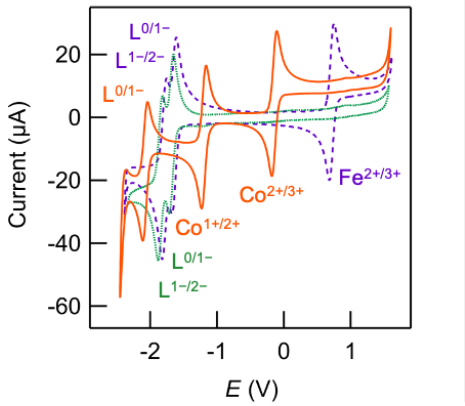

Figure S2. Overlaid solution cyclic voltammograms of parent [M(**tpy**)$_2$](PF$_6$)$_2$ complexes, showing salient features. M = Fe (purple dashed, current scaled by 0.6), Co (orange solid), Zn (green dotted). Features assigned based on previous reports.[16]

Table S9. Selected solution electrochemical parameters for metal bis(terpyridine) complexes.[a]

entry	complex	process	$E_{1/2}$	ΔE_p	E_{pa}	E_{pc}	I_{pa}/I_{pc}
1	[Fe(tpy)$_2$][PF$_6$]$_2$	$M^{2+/3+}$	0.716	0.068	0.750	0.682	1.10
2	**FeSS**	$M^{2+/3+}$	0.683	0.066	0.716	0.650	1.00
3	[Co(tpy)$_2$][PF$_6$]$_2$	$M^{2+/3+}$	−0.143	0.063	−0.112	−0.175	1.00
		$M^{1+/2+}$	−1.187	0.059	−1.158	−1.217	0.96
4	**CoSS**	$M^{2+/3+}$	−0.152	0.067	−0.119	−0.186	0.99

[a] Conditions: scan rate 0.1 V s^{-1}; working electrode, glassy carbon; reference and counter electrodes, Pt; electrolyte, MeCN−0.1 M Bu$_4$NPF$_6$. All potentials in V, corrected for iR_s and reported relative to FcH/[FcH]$^+$. $\Delta E_p = | E_{pa} - E_{pc} |$.

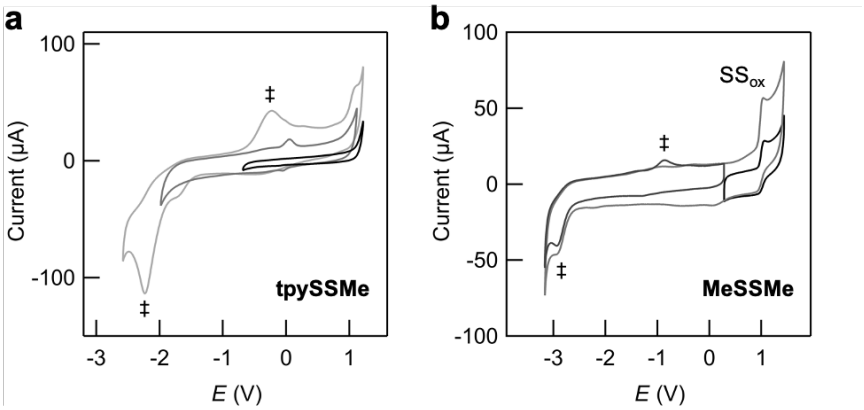

Figure S3. Representative overlaid solution cyclic voltammograms of **(a) tpySSMe** in CH_2Cl_2−0.1 M Bu_4NPF_6 and **(b)** dimethyldisulfide (**MeSSMe**) in MeCN−0.1 M Bu_4NPF_6. Potentials for voltammograms without redox features are adjusted relative to other voltammograms obtained during the same experiment, and may exhibit errors up to ±0.1 V due to reference potential drift. Redox features marked by double-daggers (‡) are attributed to the reduction of the disulfide group (SS_{red}), followed by oxidation of the resulting thiolate(s) to thiyl radicals (S^{-}_{ox}, **Figure 3e**).[17] For **MeSSMe**, the oxidation feature marked by "SS_{ox}" is attributed to the formation of a disulfide radical cation (R−$SS^{+\cdot}$−R).

Table S10. Selected electrochemical parameters for disulfide-based redox processes.[a]

entry	complex	$E_{(SSred)}$	$E_{(S-ox)}$ [b]	$E_{(SSox)}$	$E_{(*,ox)}$	$E_{(*,red)}$
1	[Fe(**tpySSMe**)$_2$][PF_6]$_2$	−1.529	(−0.31)	-	1.021	−1.079
2	[Co(**tpySSMe**)$_2$][PF_6]$_2$	−1.07 [c]	(0.52)	-	1.036	−0.898
3	[Zn(**tpySSMe**)$_2$][PF_6]$_2$	−1.542	(0.37)	-	1.040	−1.111
5	**tpySSMe** [d]	−2.236	−0.247	-	-	-
			(−0.63)			
6	**MeSSMe**	−2.928	−0.869	1.029	-	-
			(−1.07)	-	-	-

[a] Conditions: scan rate 1 V s^{-1}; working electrode, glassy carbon; reference and counter electrodes, Pt; electrolyte, MeCN−0.1 M Bu_4NPF_6, unless otherwise stated. All potentials in V, corrected for iR_s and reported relative to FcH/$[FcH]^+$. [b] Obtained from voltammograms extending to reduction potentials below the SS_{red} feature. Values in parentheses are the onset potential. [c] Onset potential. [d] Measured in CH_2Cl_2–0.1 M Bu_4NPF_6 due to the poor solubility of this compound in MeCN.

Table S11. Selected electrochemical parameters for **MSS**, and **CoSH** SAMs.[a]

entry	SAM (ratio/conditions)	$M^{2+/3+}$	$E_{1/2}$	ΔE_p	E_{pa}	E_{pc}	I_{pa}/I_{pc}[b]	E_{FWHM} [c]	**Γ** (pmol/cm^2) [c]
1	**FeSS**	Fe	0.823	0.080	0.863	0.783	0.61	0.191	33.85
2	**CoSS**	Co	−0.105	0.060	−0.075	−0.135	0.92	0.211	39.46 [d]
3	**CoSS** (N_2) [e]	Co	−0.108	0.042	−0.087	−0.129	0.85	0.232	52.29
4	**CoSH** (N_2) [e]	Co	−0.072	0.042	−0.051	−0.093	0.84	0.180	39.88
5	**CoSS** (Au-on-glass) [f]	Co	−0.085	0.126	−0.022	−0.148	0.78	0.332	43.50

[a] Conditions: scan rate 1 V s^{-1}; working electrode, chemically modified Au disc; reference and counter electrodes, Pt; electrolyte, CH_2Cl_2−0.1 M Bu_4NPF_6, unless otherwise stated. All potentials in V, corrected for iR_s and reported relative to FcH/[FcH]$^+$. $\Delta E_p = | E_{pa} - E_{pc} |$. [b] We attribute deviations from $I_{pa}/I_{pc} = 1$ for **MSS** and **MSH** SAMs to difficulties in accurately fitting baselines to these low intensity voltammogram peaks, particularly for peaks close to the onset of solvent oxidation. [c] Average full width at half maximum (E_{FWHM}) and surface coverage (**Γ**) obtained by analysis of both oxidation and reduction waves. [d] Average from 6 electrodes. [e] SAMs prepared under N_2 in a glovebox. [f] SAMs prepared on "as deposited" gold-on-glass substrates with a geometric area of 1.1 cm^2. Potentials reported for scan rate 0.1 V s^{-1}.

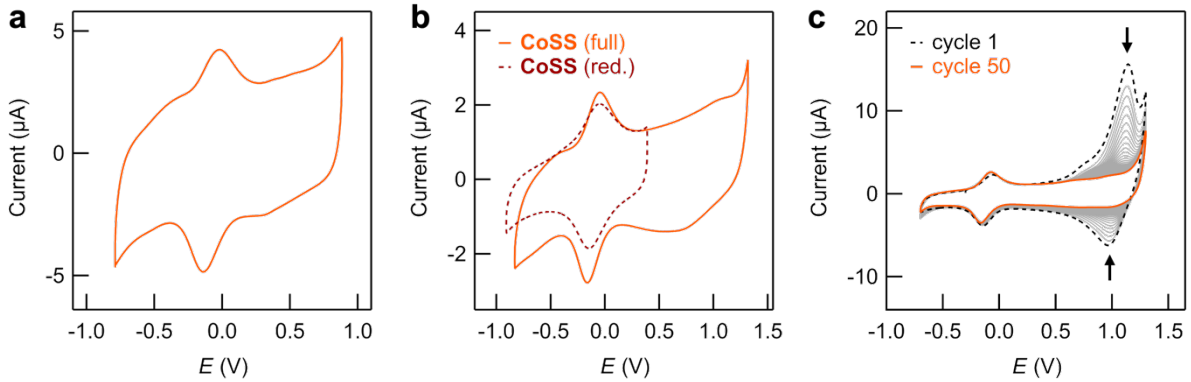

Figure S4. (a) A cyclic voltammogram obtained for a **CoSS** SAM formed on a freshly evaporated gold-on-glass substrate, with potentials corrected for iR_s. The surface coverage is comparable to SAMs prepared on gold disc electrodes, indicating the surface composition of these SAMs is broadly independent of the electrode surface roughness (**Table S11**). We attribute the high apparent ΔE_p and E_{FWHM} for this SAM (**Table S11**) to uncompensated resistances associated with the use of a large area working electrode in CH_2Cl_2-0.1 M Bu_4NPF_6. **(b)** Overlaid cyclic voltammograms for the same **CoSS** SAM as shown in **Figure 4b**, scanned to different potentials. The double-layer capacitance of these modified electrodes is reduced when scanning to potentials below the oxidative limit (extended potential range voltammogram reproduced from **Figure 4b** for convenience). **(c)** We plot representative overlaid surface cyclic voltammograms measured in CH_2Cl_2–0.1 M Bu_4NPF_6 for a SAM formed from an acetone solution of a **CoSS** sample prepared using method A (cycle 1 = black dotted, cycle 50 = orange solid). A distinct irreversible oxidation feature is observed that disappears upon repeated potential cycling. These voltammograms are representative of SAMs formed from solutions of this **CoSS** sample in MeCN for ≥18 h or 2 h, from a MeCN solution of $\mathbf{CoSS^{3+}}$ prepared from this **CoSS** sample, or for analogous SAMs measured in MeCN–0.1 M Bu_4NPF_6. No obvious impurities were observed by ^{1}H NMR spectroscopy, and elemental analysis of this sample agreed with the calculated CHN% values.

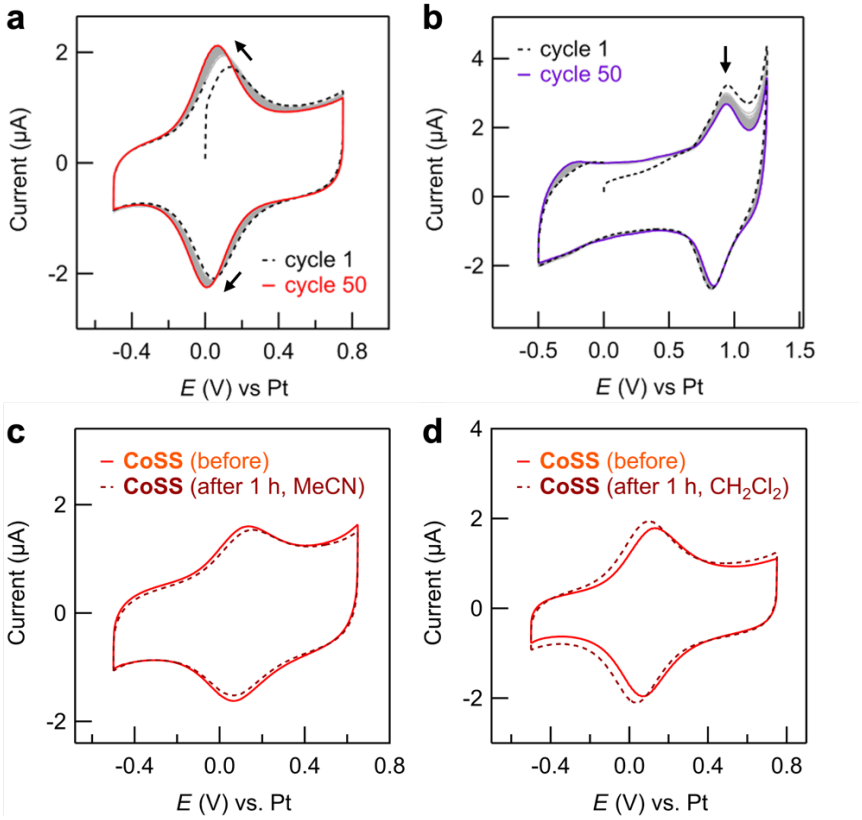

Figure S5. (a, b) Overlaid cyclic voltammograms for **CoSS** and **FeSS** SAMs, respectively, showing the current response upon repeated potential cycling in CH_2Cl_2 (cycle 1 = black dotted; cycle 100 = orange/purple solid). No significant reduction in the peak intensity is observed, indicating these SAMs are stable upon repeated oxidation/reduction. **(c, d)** Overlaid cyclic voltammograms for **CoSS**-functionalized electrodes measured before (solid) and after (dotted) immersion for 1 h in CH_2Cl_2 or MeCN, respectively, indicate limited SAM desorption on timescales relevant for electrochemical analyses. Small changes in peak intensity correlate with changes in the double-layer capacitance, suggesting the SAMs may be reorganizing on the surface over time.

7. NMR Spectra

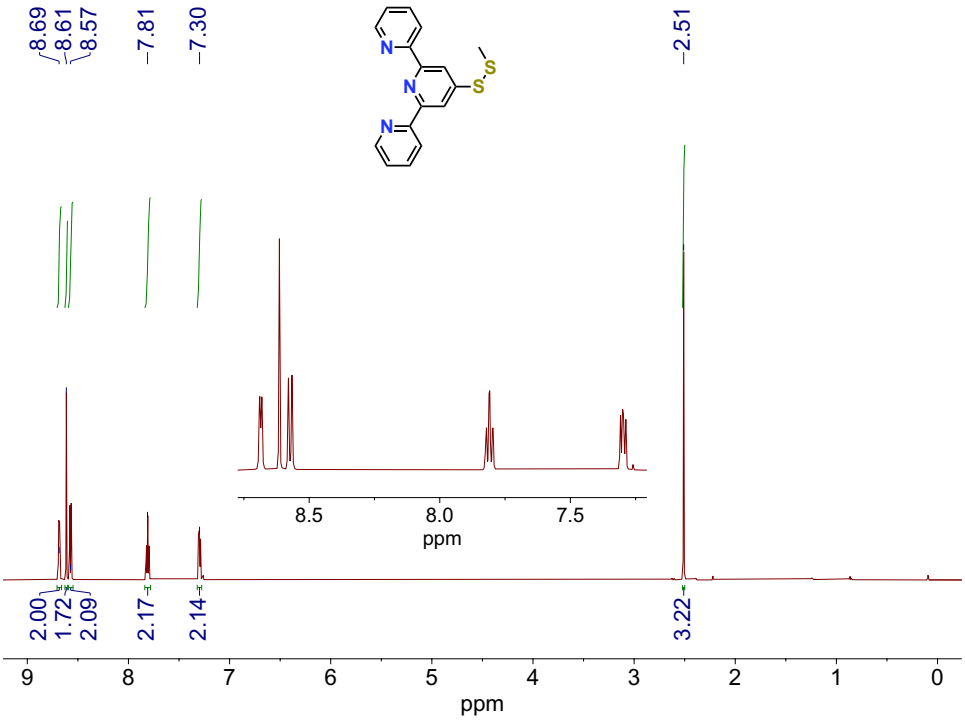

Figure S6. ^{1}H NMR (600 MHz) spectrum of **tpySSMe** in $CDCl_3$.

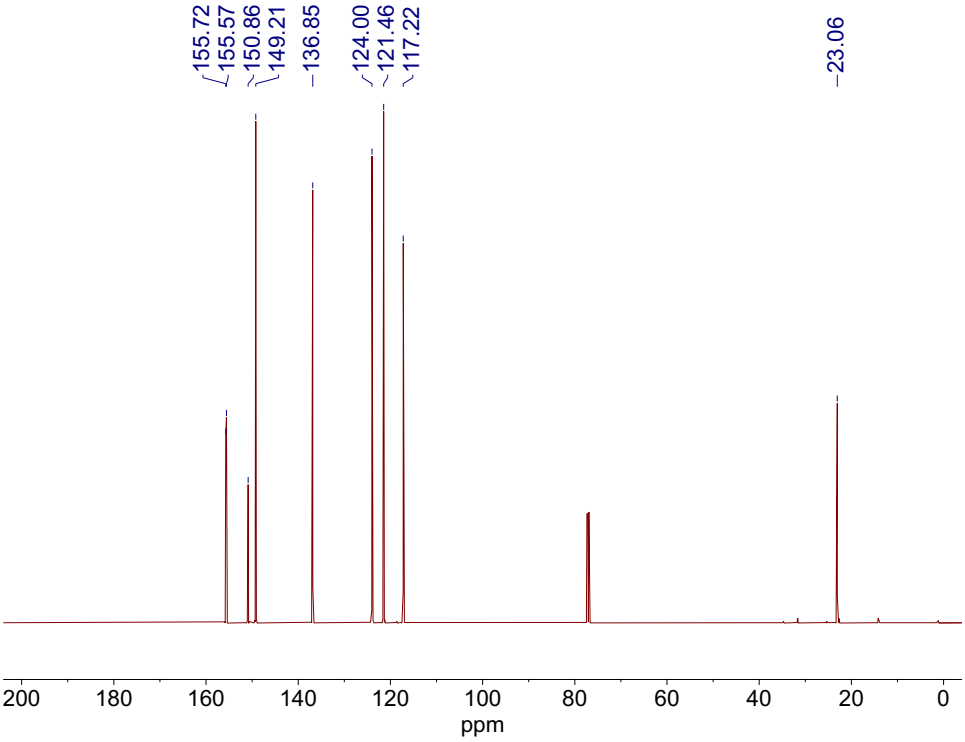

Figure S7. ^{13}C{^{1}H} NMR (150 MHz) spectrum of **tpySSMe** in $CDCl_3$.

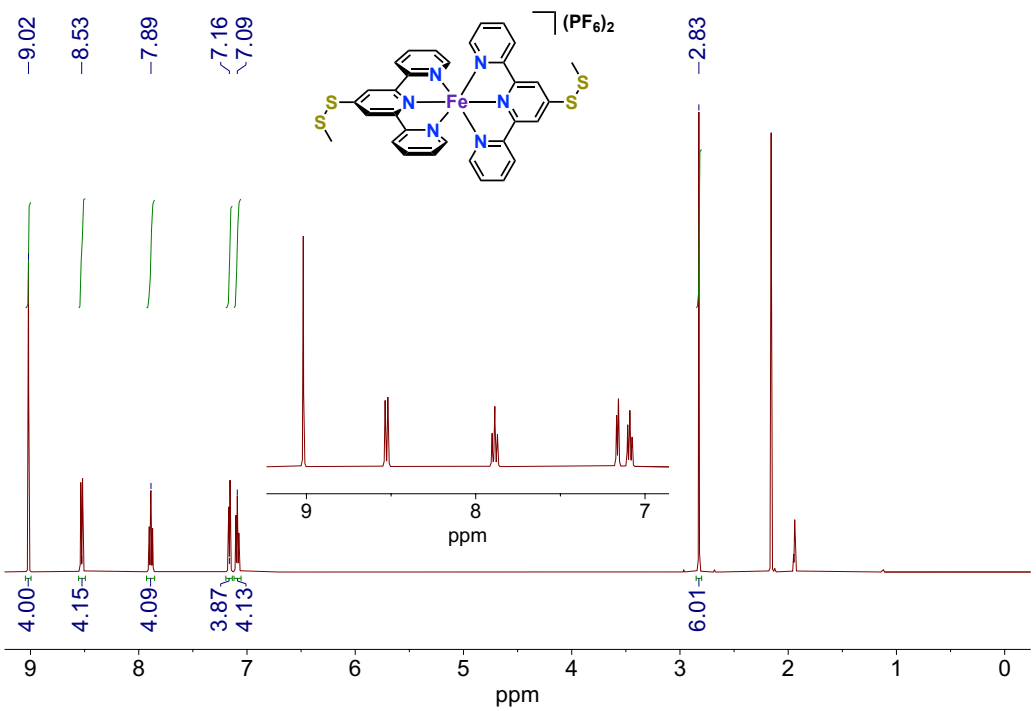

Figure S8. ^{1}H NMR (500 MHz) spectrum of **FeSS** in MeCN-d_3.

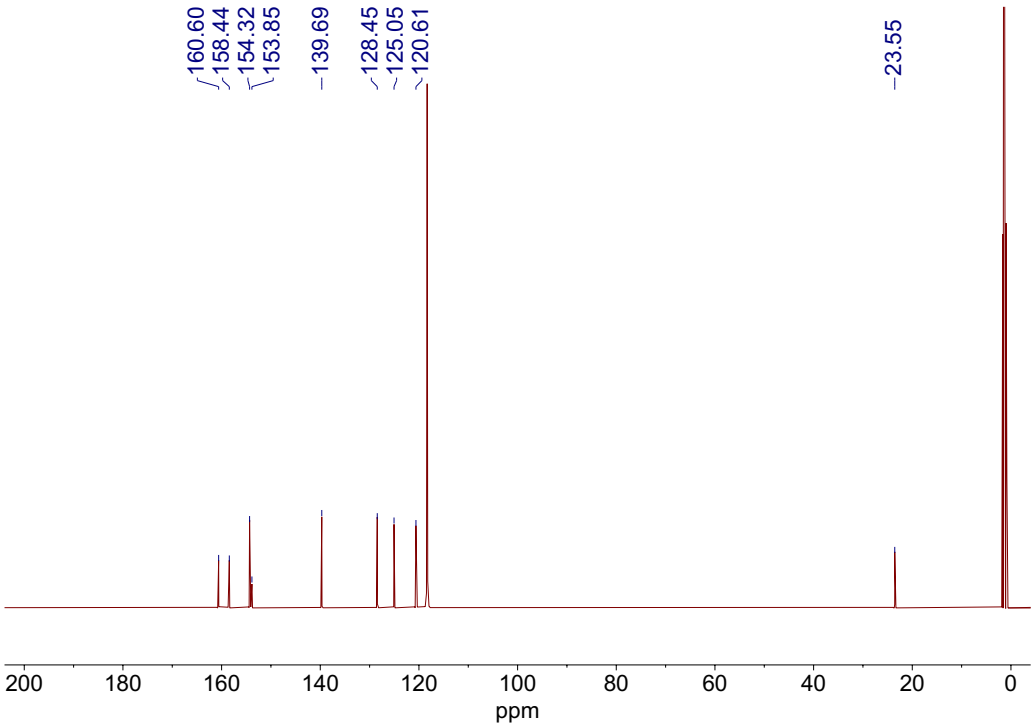

Figure S9. ^{13}C{^{1}H} NMR (125 MHz) spectrum of **FeSS** in MeCN-d_3.

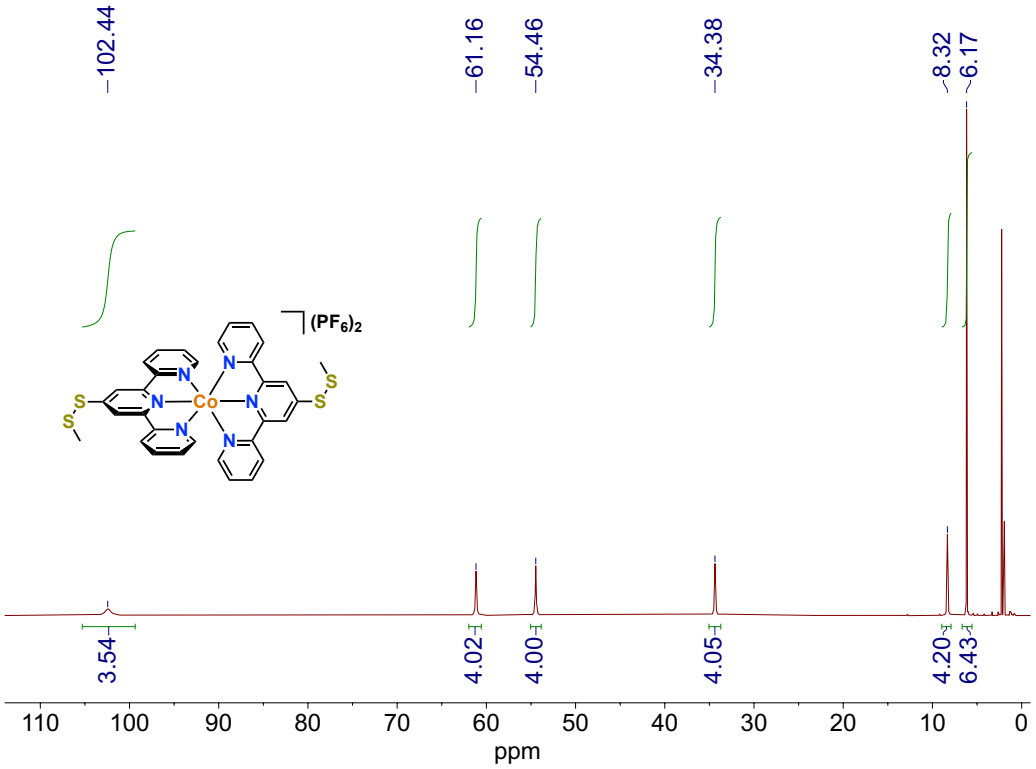

Figure S10. ^{1}H NMR (400 MHz) spectrum of **CoSS** in MeCN-d_3.

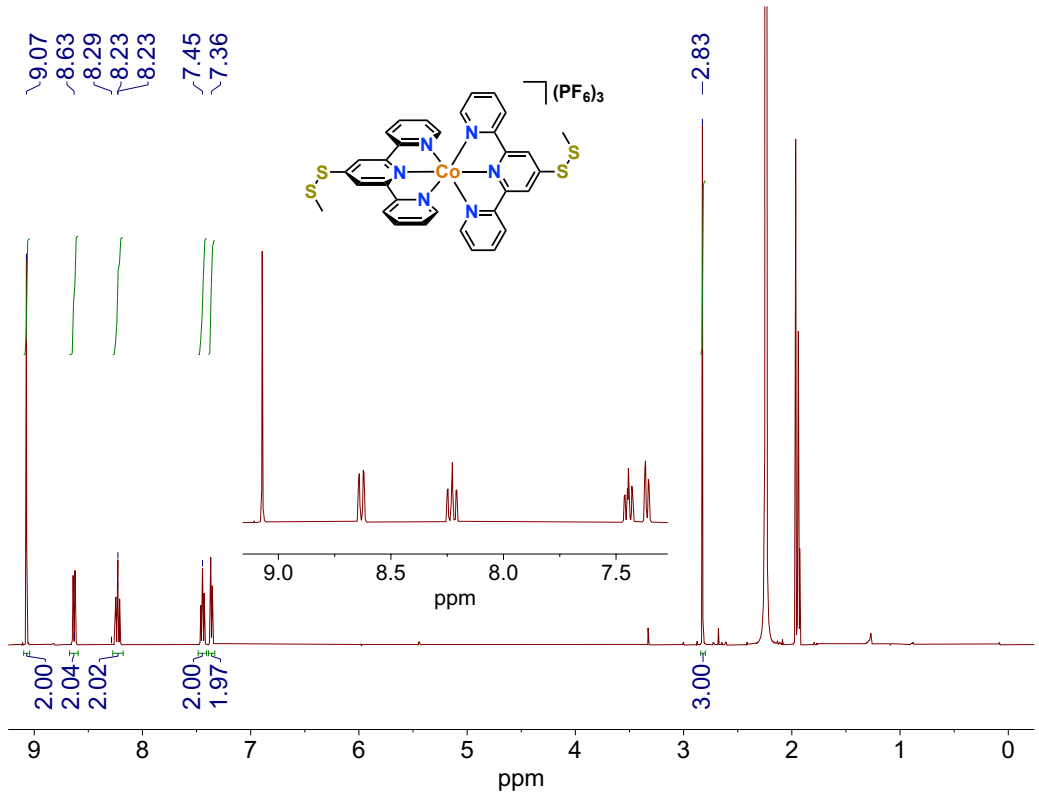

Figure S11. ^{1}H NMR (400 MHz) spectrum of **CoSS^{3+}** in MeCN-d_3.

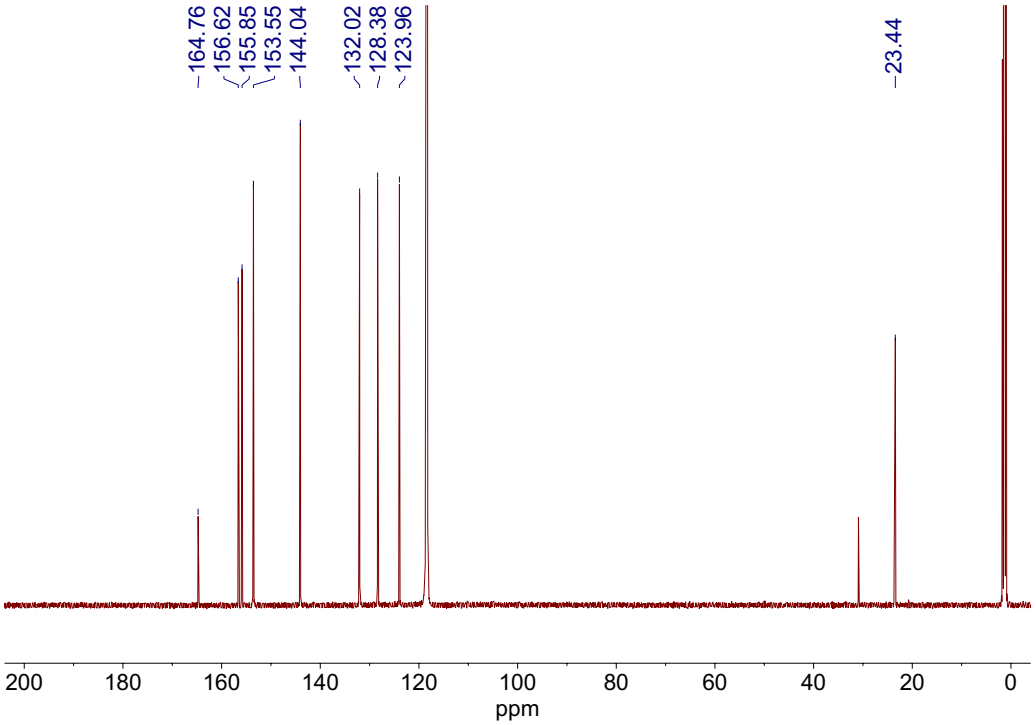

Figure S12. $^{13}C\{^{1}H\}$ NMR (150 MHz) spectrum of **CoSS**$^{3+}$ in MeCN-d_3.

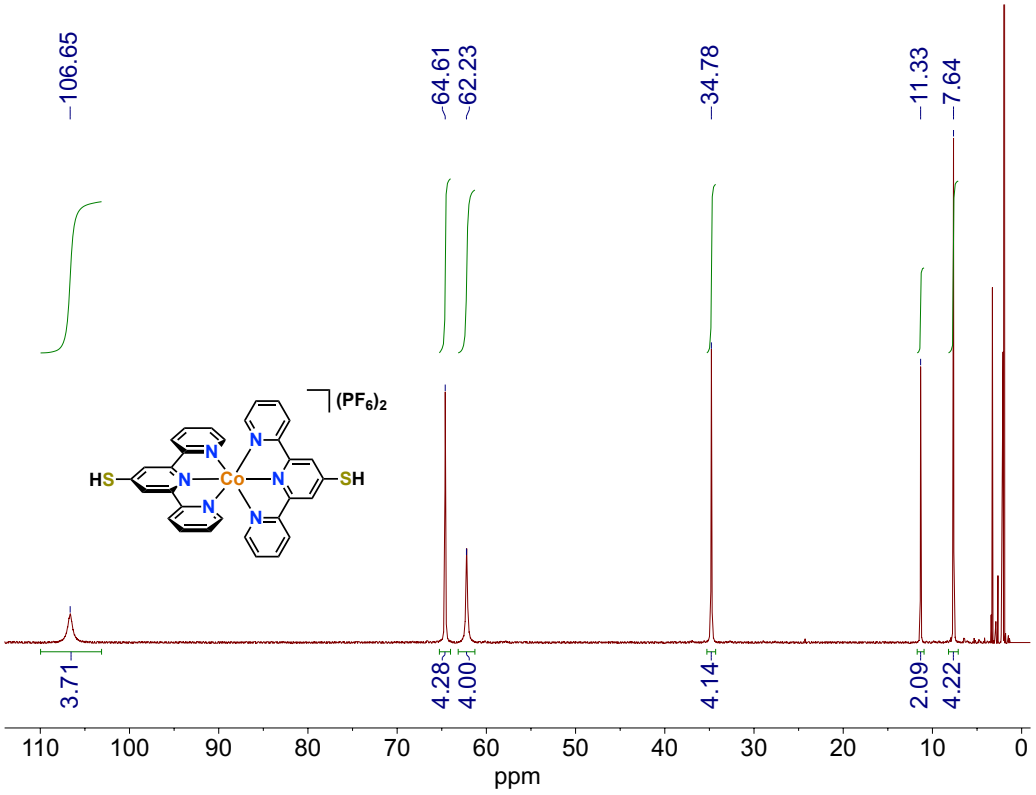

Figure S13. ^{1}H NMR (500 MHz) spectrum of **CoSH** in MeCN-d_3 (under N_2 atmosphere).

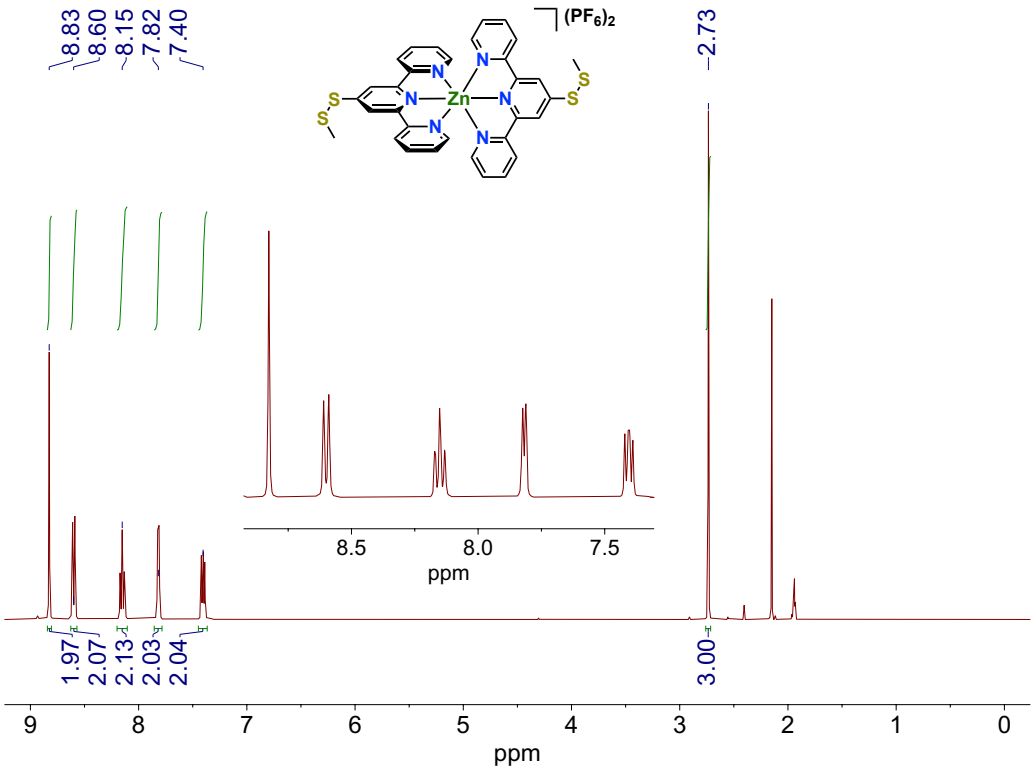

Figure S14. ^{1}H NMR (600 MHz) spectrum of **ZnSS** in MeCN-d_3.

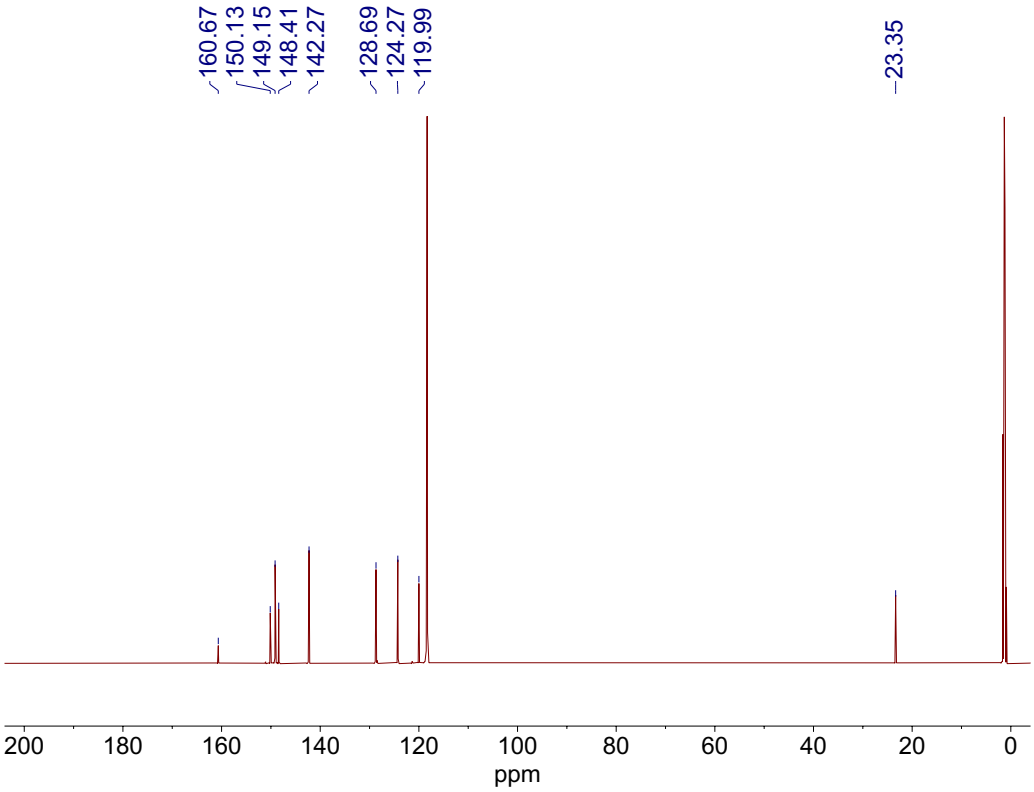

Figure S15. ^{13}C{^{1}H} NMR (150 MHz) spectrum of **ZnSS** in MeCN-d_3.

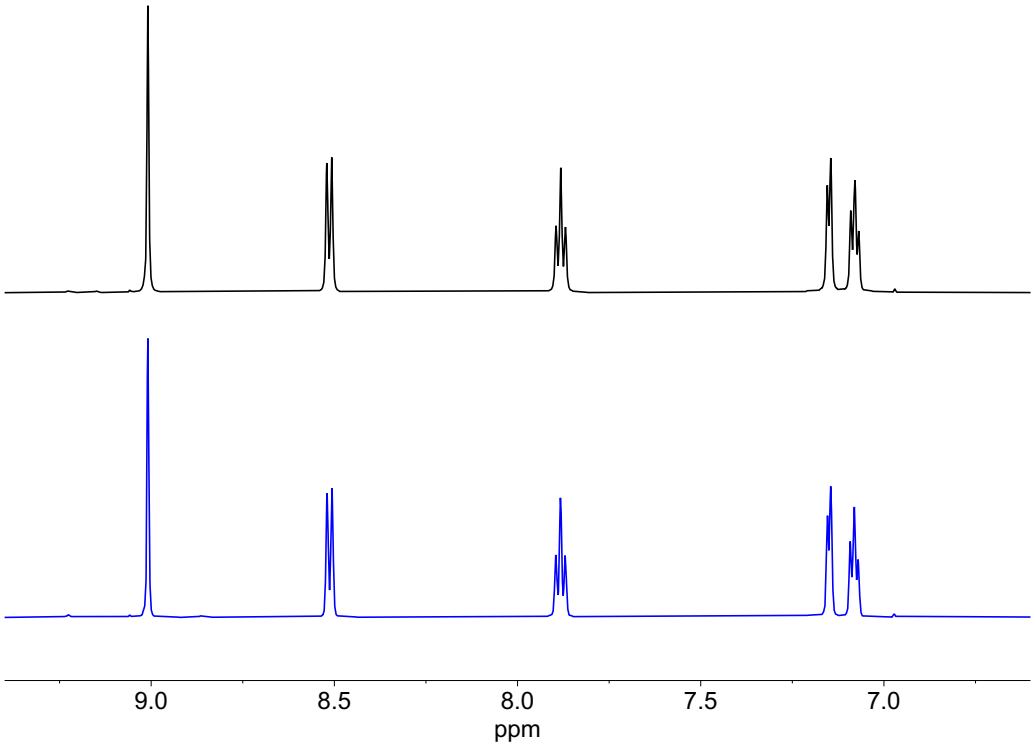

Figure S16. Stacked ^{1}H NMR (600 MHz) spectra for **FeSS** in MeCN-d_3 measured in air, expanded to show the aromatic region. The spectrum obtained after 7 d (*bottom*) shows no discernible changes compared to the initial spectrum (*top*). This confirms that **FeSS** exhibits a higher solution stability relative to **FeSH**, which is reported to form disulfide-bridged multinuclear complexes in air after 1 d.[18]

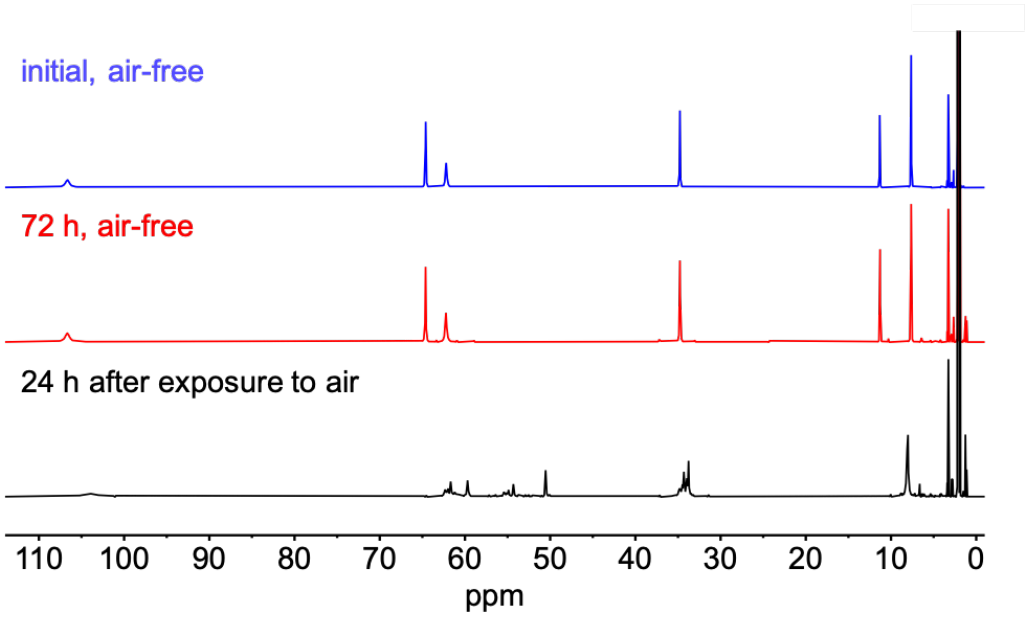

Figure S17. Stacked ^{1}H NMR spectra (500 MHz) for **CoSH** in MeCN-d_3. No significant spectral changes are observed after 72 h (blue, red) for a sample prepared in the glovebox and stored in a sealed NMR tube, indicating **CoSH** does not readily decompose in air-free solution. A processed spectrum is shown in **Figure S11**. After exposure of the same sample to air for 24 h, substantial changes to the characteristic **CoSH** ^{1}H NMR resonances are observed providing strong evidence of the compound's rapid decomposition (black, bottom).

8. References

(1) Fulmer, G. R.; Miller, A. J. M.; Sherden, N. H.; Gottlieb, H. E.; Nudelman, A.; Stoltz, B. M.; Bercaw, J. E.; Goldberg, K. I. NMR Chemical Shifts of Trace Impurities: Common Laboratory Solvents, Organics, and Gases in Deuterated Solvents Relevant to the Organometallic Chemist. *Organometallics* **2010**, *29*, 2176–2179.

(2) SHELXTL 2014/7, Bruker AXS, Madison, WI, 2014.

(3) Sheldrick, G. M. SHELX-97. *Acta Crystallogr., Sect. A* **2008**, *64*, 112–122.

(4) Sheldrick, G. M. Crystal Structure Refinement with SHELXL. *Acta Crystallogr., Sect. C* **2015**, *71*, 3–8.

(5) Hübschle, C. B.; Sheldrick, G. M.; Dittrich, B. ShelXle: A Qt Graphical User Interface for SHELXL. *J. Appl. Crystallogr.* **2011**, *44*, 1281–1284.

(6) CrysAlisPro. Rigaku, V1.171.41.120a, 2021.

(7) Ron, H.; Matlis, S.; Rubinstein, I. Self-Assembled Monolayers on Oxidized Metals. 2. Gold Surface Oxidative Pretreatment, Monolayer Properties, and Depression Formation. *Langmuir* **1998**, *14*, 1116–1121.

(8) Trasatti, S.; Petrii, O. A. Real Surface Area Measurements in Electrochemistry. *J.Electroanal. Chem.* **1992**, *327*, 353–376.

(9) Zuliani, C.; Walsh, D. A.; Keyes, T. E.; Forster, R. J. Formation and Growth of Oxide Layers at Platinum and Gold Nano- and Microelectrodes. *Anal. Chem.* **2010**, *82*, 7135–7140.

(10) Constable, E. C.; Hermann, B. A.; Housecroft, C. E.; Neuburger, M.; Schaffner, S.; Scherer, L. J. 2,2′:6,2″-Terpyridine-4′(1′H)-Thione: A Missing Link in Metallosupramolecular Chemistry. *New J. Chem.* **2005**, *29*, 1475–1481.

(11) Kitson, T. M.; Loomes, K. M. Synthesis of Methyl 2- and 4-Pyridyl Disulfide from 2- and 4-Thiopyridone and Methyl Methanethiosulfonate. *Anal. Biochem.* **1985**, *146*, 429–430.

(12) Harzmann, G. D.; Neuburger, M.; Mayor, M. 4,4″-Disubstituted Terpyridines and Their Homoleptic Fe^{II} Complexes. *Eur. J. Inorg. Chem.* **2013**, *2013*, 3334–3347.

(13) Constable, E. C.; Housecroft, C. E.; Kulke, T.; Lazzarini, C.; Schofield, E. R.; Zimmermann, Y. Redistribution of Terpy Ligands—Approaches to New Dynamic Combinatorial Libraries. *J. Chem. Soc. Dalt. Trans.* **2001**, No. 19, 2864–2871.

(14) Chambers, J.; Eaves, B.; Parker, D.; Claxton, R.; Ray, P. S.; Slattery, S. J. Inductive

Influence of 4′-Terpyridyl Substituents on Redox and Spin State Properties of Iron(II) and Cobalt(II) Bis-Terpyridyl Complexes. *Inorganica Chim. Acta* **2006**, *359*, 2400–2406.

(15) Gryko, D. T.; Clausen, C.; Roth, K. M.; Dontha, N.; Bocian, D. F.; Kuhr, W. G.; Lindsey, J. S. Synthesis of "Porphyrin-Linker-Thiol" Molecules with Diverse Linkers for Studies of Molecular-Based Information Storage. *J. Org. Chem.* **2000**, *65*, 7345–7355.

(16) Dickenson, J. C.; Haley, M. E.; Hyde, J. T.; Reid, Z. M.; Tarring, T. J.; Iovan, D. A.; Harrison, D. P. Fine-Tuning Metal and Ligand-Centered Redox Potentials of Homoleptic Bis-Terpyridine Complexes with 4′-Aryl Substituents. *Inorg. Chem.* **2021**, *60*, 9956–9969.

(17) Borsari, M.; Cannio, M.; Gavioli, G. Electrochemical Behavior of Diphenyl Disulfide and Thiophenol on Glassy Carbon and Gold Electrodes in Aprotic Media. *Electroanalysis* **2003**, *15*, 1192–1197.

(18) Van Der Geer, E. P. L.; Van Koten, G.; Klein Gebbink, R. J. M.; Hessen, B. A [4Fe-4S] Cluster Dimer Bridged by Bis(2,2′:6′,2″- Terpyridine-4′-Thiolato)Iron(II). *Inorg. Chem.* **2008**, *47*, 2849–2857.